DESIGN OF A DROP-ON-DEMAND DELIVERY SYSTEM FOR MOLTEN SOLDER MICRODROPS

by

GREGG MICHAEL DUTHALER

B.S.E. in Mechanical Engineering, Princeton University, 1992

Submitted to the Department of Mechanical Engineering
in Partial Fulfillment of the Requirements
for the Degree of

Master of Science
in Mechanical Engineering

at the

MASSACHUSETTS INSTITUTE OF TECHNOLOGY

January 1995

Signature of Author _____
Department of Mechanical Engineering

Certified by _____
Ain A. Sonin
Professor, Mechanical Engineering
Thesis Supervisor

Accepted by _____
Ain A. Sonin
Chairman, Departmental Committee on Graduate Studies
Department of Mechanical Engineering

DESIGN OF A DROP-ON-DEMAND DELIVERY SYSTEM FOR MOLTEN SOLDER MICRODROPS

by

GREGG MICHAEL DUTHALER

Submitted to the Department of Mechanical Engineering
on January 20, 1995 in partial fulfillment
of the requirements for the degree of
Master of Science in Mechanical Engineering

ABSTRACT

This project aims to develop an understanding of the fundamental physics governing the design and performance of a drop-on-demand microdrop (approximately 50 μm diameter) delivery system for molten solder. The preliminary examination of a range of design concepts illustrates the feasibility of producing such a system and leads to the selection of a design for further development. Basic theory is used to develop several mock-ups of the proposed device. After preliminary experimentation a more complete mathematical model of the ejection system is developed. Numerically solving the derived governing equations allows prediction of the performance of the system as a function of design parameters. To test the validity of the model, a prototype system is constructed and tested using water as the working fluid. After successfully operating this prototype, several design deficiencies were addressed during the development of a second system. Despite limited success in ejecting liquid mercury from this new device, it demonstrates the feasibility of the design concept for solder delivery, and serves as a stepping stone for further work involving the ejection of high temperature molten droplets of metal.

Thesis Supervisor: Dr. Ain A. Sonin

Title: Professor of Mechanical Engineering

I dedicate this thesis to my grandparents...

Listen little fellow, before you get old,
a good education is better than gold,
'cause gold and silver may fade away,
but a good education is here to stay.

ACKNOWLEDGEMENTS

A work of this magnitude can never be accomplished alone. I extend my warmest gratitude to Professor Sonin for his confidence, patience, and remarkable ability to simplify, simplify, simplify. The successful design of the system proved tougher than anticipated, and the support and guidance of my advisor helped make the frequent frustration a bit more bearable. Afterall, science still works.

I thank my family for the love, support, and no-charge design consultation during the tough times. You have given me everything, and I can only say thank you.

Thanks to Dick Fenner, who shook my hand when I finished machining that first mock-up, who taught me how to efficiently manipulate the MIT system, and whose war stories will forever echo through the hallowed halls.

I offer my deepest thanks to my colleagues, Dr. Fuguan Gao and Stefano Schiaffino, for their diligence, know-how, and friendship. Are we going to rearrange the lab area *again*?

Thanks to all my other friends in the lab who make the days go by so quickly: Edwin, for the dinners, the bike rides, the good times and the bad, and the friendship; Mariano, for going through this place before I did; Naomi and Serhat, who keep an excellent pace; Arthur and Barry, for their remarkable compassion for tragedy; James, for the late night companionship; Frank and Jim, for shooting well above par also; Manuel, who is definitely just-a-little-bit conservative; Wilson, who may someday believe that Ivy League grads can actually operate a milling machine; Dave O., who warned me about ink jet air bubbles in late 1992; California Dave, for forsaking work to see that lacrosse game; Sanjay, who shared with me my birthday rice pudding; Barbara and Kevin, for jogging up the canyon at Killington in an October snowstorm while wearing spring clothes;

Kathy, Kevin, and Baby MacKenzie, who taught me how to ride well; Dino, for quals companionship; Hugo, for buying your first pentium computer in late 1995; Amit and John O., for keeping a faster pace than Naomi and Serhat; Big John, who always took my money at poker night; and thanks to Chahid, Joseph, Chun-Hai, Dilip, Mick, Matteo, Rich, Takuya, Marius, Tim, and everyone else who I forgot to mention. You all helped make this the experience of a lifetime.

I offer my gratitude to Dr. Javier Valenzuela of Mikros Manufacturing, Randy Jezowski of RAMCO, Inc., and John Stacy of American Piezo Ceramics for their design and manufacturing advice. Also, thanks to Tad Snow and my other friends from the Advanced Engineering Design class, who showed me how it should be done.

Lastly, I extend my sincerest appreciation to Bob Pfahl of Motorola, Inc., who arranged for the financial support of this research effort.

TABLE OF CONTENTS

LIST OF FIGURES

LIST OF TABLES

CHAPTER 1

Introduction

1.1 Background

In the 1960s, IBM Corporation devised a novel system for attaching the silicon wafer to the mounting substrate of an integrated circuit package. [Davis *et al* 1964, Totta and Sopher 1969, Miller 1969] Conventionally, wire-bonding techniques were used to attach the fine wires from the land on the microchip to the pin on its package. As illustrated in Figure 1.1, the new IBM method sought to alter the paradigm of microchip assembly by placing the attachment point in between the silicon wafer and a conductive pad on the high resistance mounting substrate. Successfully accomplishing this task would shrink overall package size and allow for higher clock speeds. To make the attachment, researchers soldered dozens of conductive balls roughly 50 μm in diameter on the substrate mounting pads. After carefully positioning the wafer, a solder reflow process was used to complete the assembly.

Unfortunately, this "flip-chip" method of microchip assembly is extremely labor intensive. In an effort to speed the assembly process, manufacturers seek a means to automatically deposit several hundred solder droplets (roughly 50 to 100 μm in diameter) on a substrate. This delivery system must repeatably and precisely deliver molten material to the target, and should allow for complete flexibility in selecting a droplet pattern.

1.2 Dispensing Droplets with an Ink Jet

One tool that provides a potential means of deposition is the drop-on-demand ink

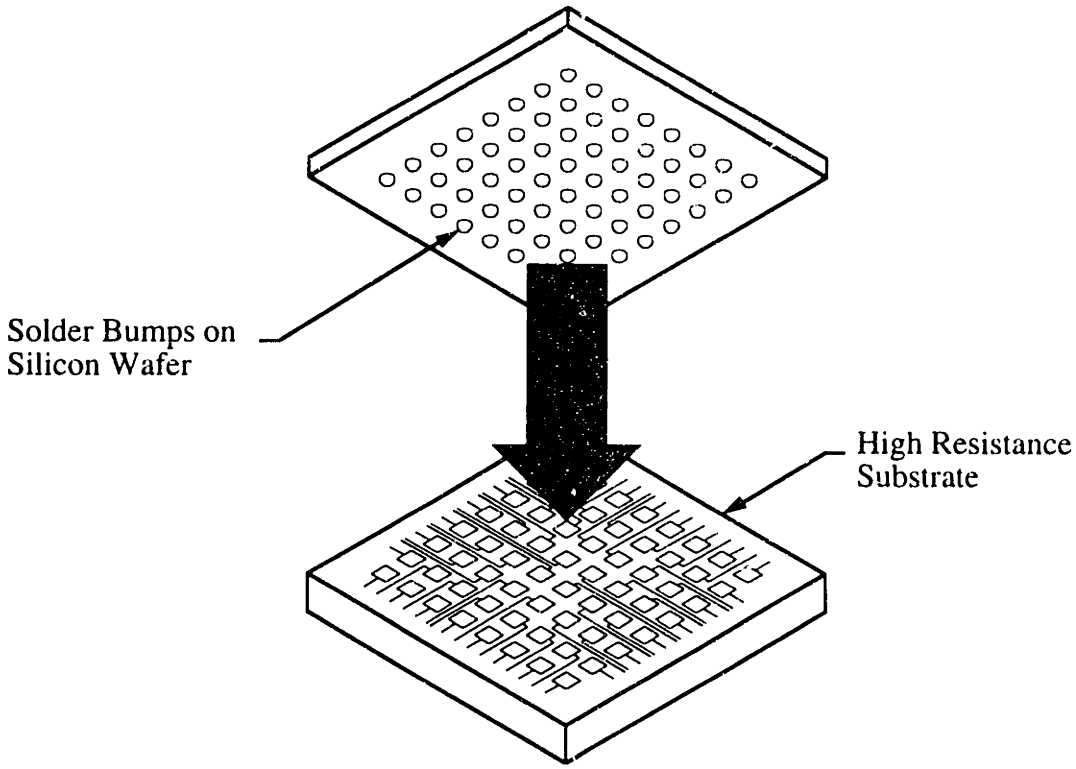

FIGURE 1.1 Flip-chip packaging uses solder bumps to make an electrical connection between the silicon wafer and the high resistance substrate.

jet, which was first developed in the late 1960s. [Kyser and Sears 1969] In these systems a single control signal causes the repeatable, ballistic ejection of a single droplet. As a molten droplet travels through the atmosphere and impacts a subcooled target, it cools and eventually solidifies. The digital nature of the device distinguishes it from a continuous jet droplet production system, in which a stream of fluid degenerates into a train of droplets. (Figure 1.2) This break-up phenomena is governed by the Rayleigh instability mechanism [Rayleigh 1878] or by external forcing. For manufacturing processes where precise, single droplet deposition is required, the drop-on-demand system is inherently more suitable than a continuous jet device. The prospects for using drop-on-demand systems for electronics packaging applications, rapid prototyping, free-form fabrication, and materials processing were explored by Gao in 1994.

A drop-on-demand system is designed so that the user simply "pushes a button"

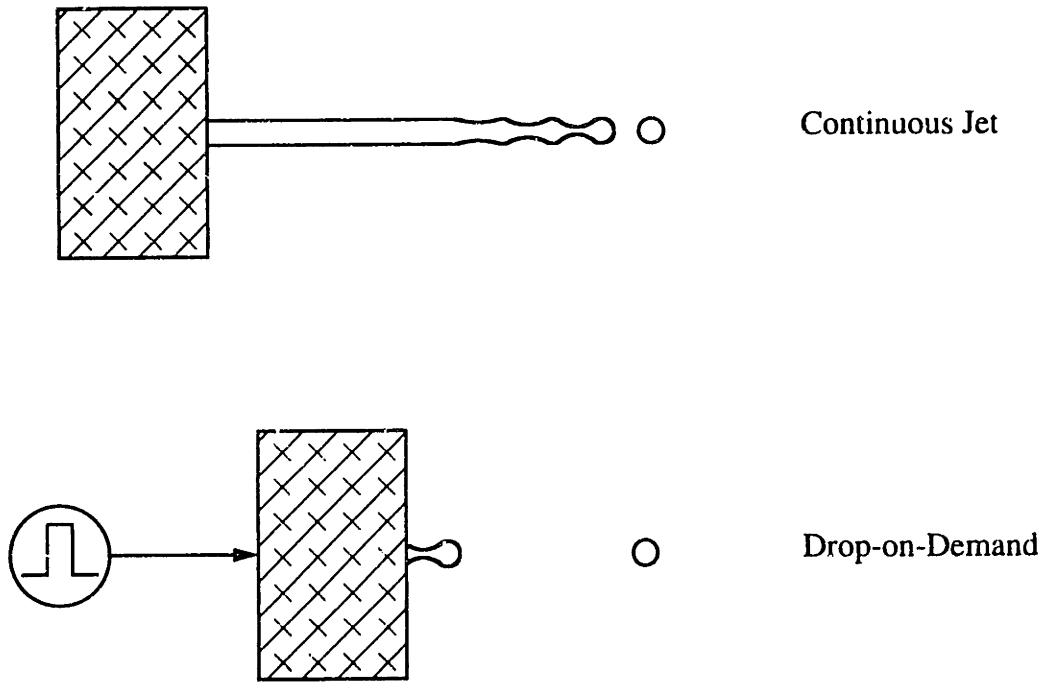

FIGURE 1.2 The continuous jet system forms a fluid stream which breaks up into droplets, while the drop-on-demand system ejects a single droplet in response to an input signal.

to eject a droplet two-thirds the diameter of a human hair. (See Figure 1.3) What remains hidden from the user makes the design challenging. The design solution depends significantly on the fluid density, surface tension, compressibility, viscosity, and, if molten metals are involved, the oxidation rate. Component geometry and design implementation are also extremely important in determining the success or failure of the design. During this research effort, for example, the imperfect clamping of a fluid chamber and the presence of air bubbles in the system proved to be especially vexing problems.

Existing ink-jet systems cannot be used to deliver solder droplets for two primary reasons: the melting point of eutectic solder exceeds the maximum allowable operating temperature of available devices, and the systems are not designed to generate the pressures required to eject the dense liquid metal. For example, Dataproducts and Tektronix manufacture molten wax printers which have maximum operating temperatures significantly below the 183°C melting point of eutectic solder. The temperature

limitations result from the use of certain piezoelectric materials, epoxies, and/or electronic components on the heated print head assembly. The second problem is a fundamental one, and requires a complete re-evaluation of the relationships among the drop-on-demand design parameters and variables.

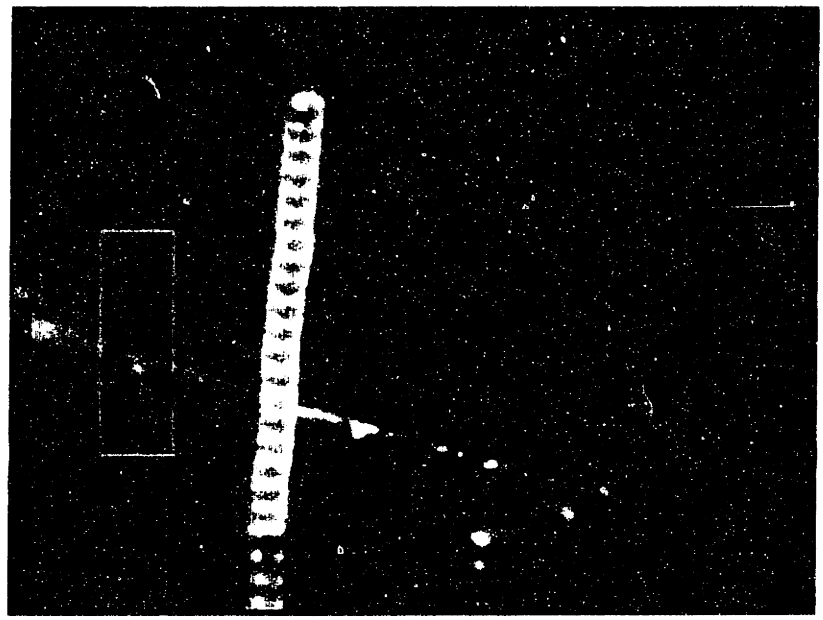

FIGURE 1.3 A human hair is as large in diameter as an ejected droplet

1.3 Objectives

This work focuses on the design and development of a device which delivers molten solder droplets of approximately 50 μm diameter on demand. Emphasis is placed upon gaining a sound understanding of the fundamental physical principles that characterize the system. Simple theoretical models are used to develop an understanding of the scaling laws intrinsic to the ejection process and the design itself. Hardware is contructed and tested in an attempt to validate the theoretical results. Throughout this research effort, strong priorities are placed on overall design simplicity and flexibility.

CHAPTER 2

Basic Design Considerations

2.1 The Ejection of Fluid through a Microscopic Orifice

A drop-on-demand system consists of a liquid supply reservoir connected to a small chamber which may be pressurized on demand to force a droplet to eject from the microscopic orifice. To illustrate the technical issues associated with such a system, consider the transient flow of an inviscid fluid through a small circular orifice cut through a thin metal sheet as depicted in cross section in Figure 2.1. The fluid density and surface tension values are denoted by ρ and σ, respectively. Imagine further that the hole diameter $2a_0$ is small enough, say of the order of tens of microns, so that surface tension forces are important.

When the pressure P(t) of the chamber fluid rises, the meniscus will accelerate outward at velocity $U_0(t)$. The meniscus forms a spherical cap at time $t = t^*$, and the pressure difference across this curved surface[&] reaches the maximum value

$$\Delta P = \frac{2\sigma}{a_o} \tag{2.1}$$

Ballistic ejection requires that the inertia of the slug at least obey

$$\frac{1}{2}\rho U_o^2(t^*) > \frac{2\sigma}{a_o} \tag{2.2}$$

[&] The pressure difference across a curved surface is described by Young's equation, which relates the principle radii of curvature to the pressure difference according to $\Delta P = \sigma(1/R_1 + 1/R_2)$. The radii may take on positive or negative values, depending upon concavity.

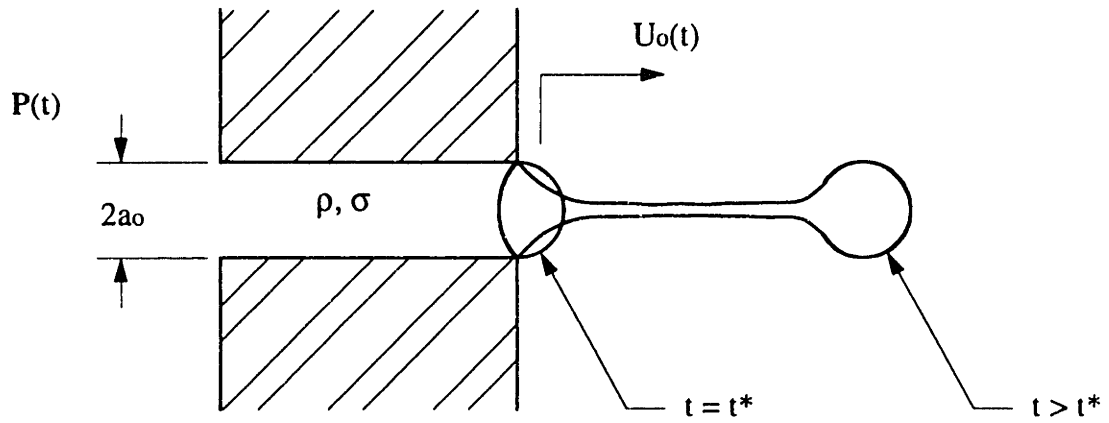

FIGURE 2.1 Ejection of fluid through a microscopic orifice of radius a_o results from an upstream pressure P. The surface tension pressure is maximum when $t = t^*$.

or in terms of the non-dimensional Weber number,

$$We = \frac{\rho U_o^2(t^*) a_o}{\sigma} > 4 \tag{2.3}$$

The inequality of Equation 2.3 is intended to serve only as an order of magnitude estimate, but does show agreement with experimental results. [Gao 1994]

The Weber number criterion is not the only design requirement for a drop-on-demand device. In order to push a single droplet of fluid out of the orifice, the volume of fluid dispensed in time of order t^* must be metered so that

$$V_{eject} = \int_0^{t^*} U_o(t)\, \pi a_o^2\, dt \sim 1 \textit{ drop volume} \tag{2.4}$$

Note that the 50 μm diameter "drop volume" is a very convenient unit which will frequently appear in this work. This simple analysis of the ejection criteria hides some

of the complexities of the actual droplet ejection process, which may be affected by fluid viscosity, and the dynamically changing shape of the fluid free surface.

The above estimates describe the compression stroke of a drop-on-demand device. As shown in Figure 2.2, the complete ejection cycle may be divided into compression, snap-off, and refill phases. Shortly after the termination of the driving pressure, the

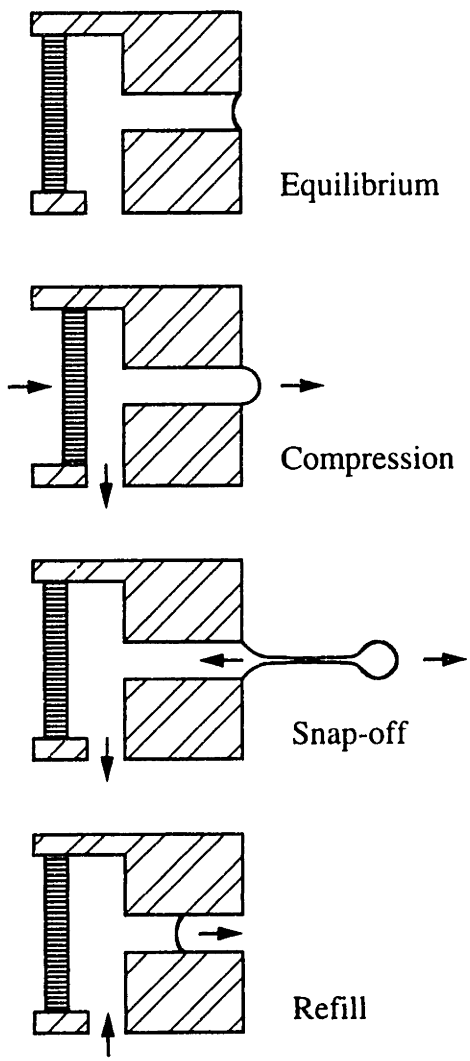

FIGURE 2.2 An impulse pump cycles through equilibrium, compression, snap-off, and refill

droplet snaps off from its connecting tail. There are three possible outcomes for the remnants of the tail: 1. some fluid is pulled directly into the droplet by surface tension forces; 2. a portion of the tail forms a small satellite droplet which catches and is engulfed by the larger droplet; and 3. material retracts back into the orifice. The subsequent replenishment of fluid to the chamber region from the reservoir is controlled by capillary and possibly hydrostatic forces.

2.2 Scales of the Design Variables

In the previous section, a simple picture of the ejection process illustrated the significance of the droplet Weber number and the time integrated volume flow rate. These same expressions can reveal valuable information about the scaling of the variables involved in this problem. In particular, Equation 2.2 may be recast as

$$U_o(t^*) > \sqrt{\frac{4\sigma}{\rho a_o}} \tag{2.5}$$

Taking the orifice radius a_o as 25 μm, and substituting property values for water (See Table 2.1) gives $U_o(t^*) = 3.4$ m/s. A minimum velocity of 2.9 m/s is required for solder ejection. A typical ejection time scale may be estimated by recognizing that the fluid has travelled through a distance approximately equal to the orifice radius when it attains the speed $U_o(t^*)$. Calculation shows the characteristic ejection time t^* is on the order of $a_o/U_o(t^*) \approx 8$ μs.

To gain an appreciation for the pressure, P, required to accelerate water to these velocities in these short times, consider the approximate momentum relation

$$P \sim \rho L_o \frac{dU_o}{dt} \tag{2.6}$$

	ρ (kg/m^3)	c (m/s)	$\kappa_s x10^{12}$ (m^2/N)	$\sigma x10^3$ (N/m)	θ_o (deg)	$\eta x10^6$ (m^2/s)	$\mu x10^4$ (Ns/m^2)
Water	996[a]	1497[b]	450	72[a]	25.5[d]	.87[a]	8.67[a]
Mercury	13530[a]	1450[b]	35	470[a]	129[d]	.11[a]	14.9[a]
Solder (63% Pb, 37% Sn)	9400[e]	2060[f]	25	500[f]	>90[g]	.26	24[h]

[a. Mills 1992, b. Weast and Astle 1980, d. Li and Lam 1976, contact angle measured on clean glass surface, e. Ashby and Jones 1986, f. Iida and Guthrie 1988, g. solder does not wet the surfaces used in this design (application of flux can improve wettability), h. Weast and Astle 1980, property estimated by weighted average of lead and tin properties evaluated at T_{melt}]

TABLE 2.1 Properties of working fluids. $\kappa_s = (\rho c^2)^{-1}$, $\eta = \mu/\rho$

Taking a typical effective orifice length L_o of 225 μm, and approximating the acceleration as $U_o(t^*)/t^*$ shows that to satisfy the Weber number criterion a constant gage pressure of about 110 kPa must act on the upstream side of the orifice. The volume flow rate integration shows that this pressure will push approximately three-eighths of a drop volume out of the orifice while $t < t^*$.

2.3 Generating a Pressure Pulse

The estimates of the previous section show that it is essential to generate and maintain a relatively large increase in fluid pressure just upstream of the orifice. Once sufficient fluid is ejected, the pressure may relax so that the system can regain its equilibrium state before the next ejection sequence. Figure 2.3 illustrates and briefly explains several design concepts that were investigated as methods for generating a pressure pulse. After careful consideration of the strengths and weaknesses of each of these ideas, it was determined that the magnetohydrodynamic and piezoelectric systems both warranted further study.

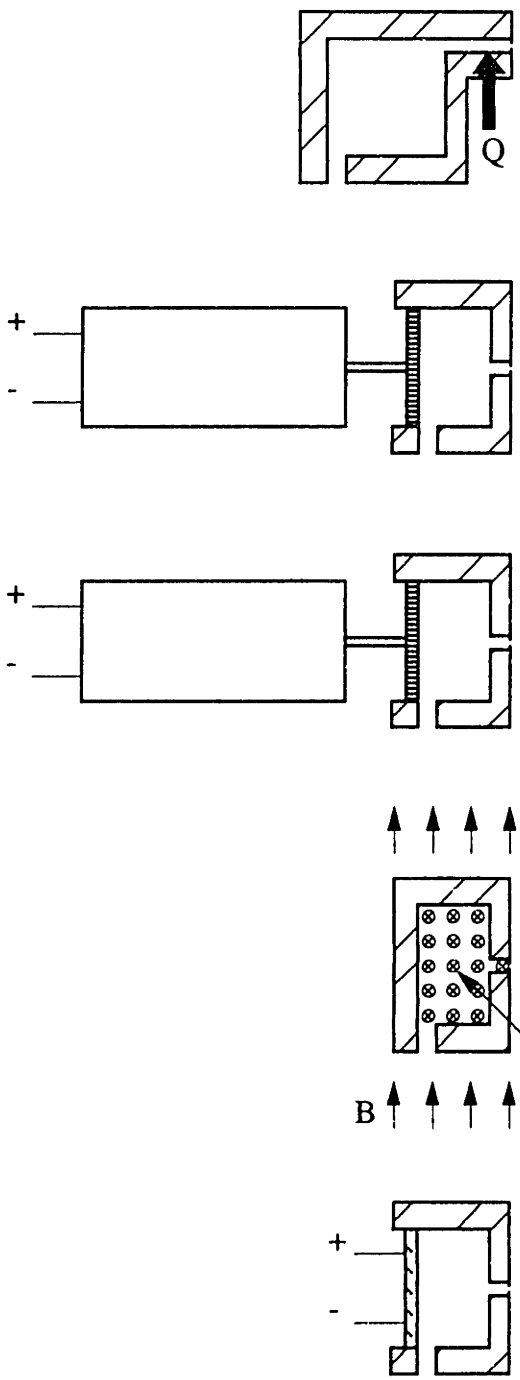

a) Heat flux causes local boiling, and the resulting vapor bubble expels the droplet.

b) The action of a solenoid pushes the droplet from the chamber.

c) A magnetostrictive actuator ejects the droplet from the chamber.

d) A crossed magnetic field and electrical current results in the magnetic pressure which accelerates the droplet.

e) A piezoelectric piston pushes the droplet from the chamber.

FIGURE 2.3 Pressure pulse generation concepts including a) local heating, b) electromechanical, c) magnetostrictive, d) magnetohydrodynamic, and e) piezoelectric.

2.3.1 Magnetohydrodynamic System

In the magnetohydrodynamic (MHD) design concept, a magnetic field is crossed in direction with an electrical current which flows through the molten conductive material. As predicted by electromagnetic theory, the vector cross product of the current density and the magnetic field describes a body force acting on the conductor. This body force will accelerate the fluid in the orifice and propel it outward.

The MHD concept is an elegant one, as the system has no moving parts whatsoever. Also, with adequate thermal protection of the magnets the device can, in principle, operate at temperatures which approach the melting temperature of its structural material. This feature may make the system well suited for the production of droplets of aluminum, copper, and other engineering materials with high melting temperatures. The working fluid is limited to materials with high electrical conductivities, and requires high currents and/or very strong magnetic fields. To better appreciate the magnitudes of some of these parameters, consider the following inviscid analysis of the MHD system depicted in Figure 2.4.

Begin by applying the unsteady integral momentum equation to a control volume enclosing the fluid between points 2 and 3 in the diagram. A uniform body force per unit volume, jB, acts on this accelerating fluid, so that

$$P_3 - P_2 = jBL_o - \rho L_o \frac{dU_o}{dt} \tag{2.7}$$

The pressures at points 1 and 2 are related by the unsteady Bernoulli equation. Taking $P_1 = P_\infty$ (atmospheric pressure), $U_1 << U_2$, and $U_2 = U_o$ shows

$$P_\infty - P_2 = \frac{1}{2}\rho U_o^2 + \rho 2h \frac{dU_o}{dt} \tag{2.8}$$

To approximately account for the acceleration of the fluid near the inlet of the orifice, two

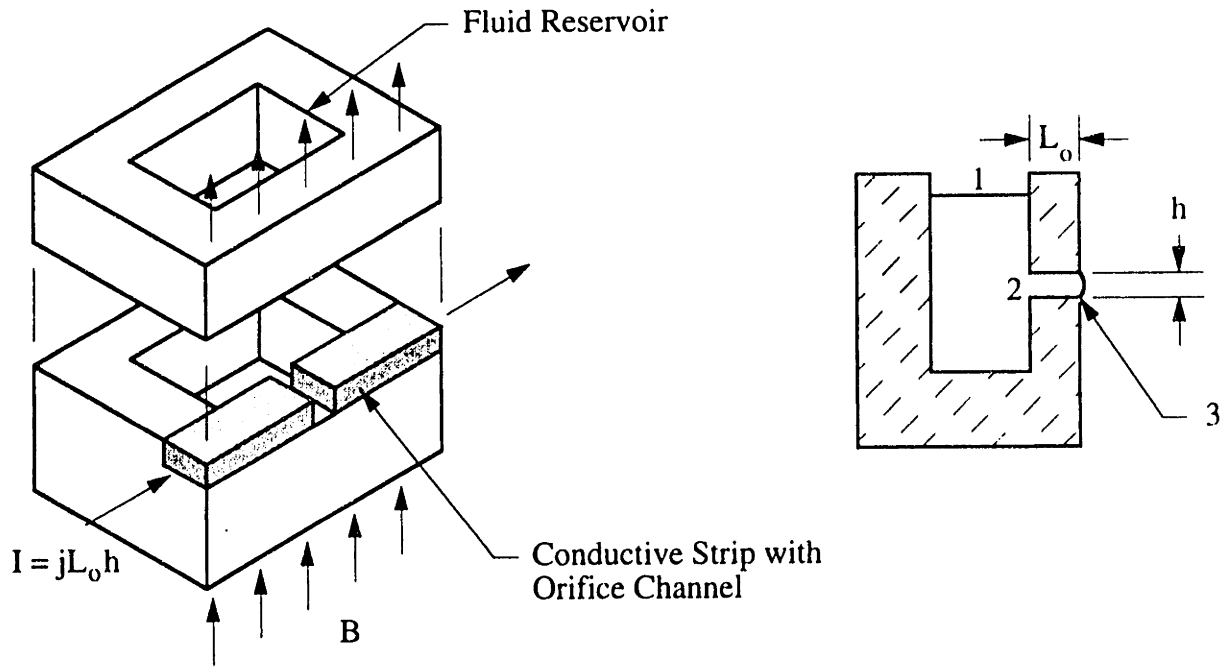

FIGURE 2.4 Isometric sketch and cross sectional view of a proposed MHD system

orifice hydraulic diameters appear in the unsteady term in this expression. (See Section 3.4 for further discussion of this approximation) To keep this analysis as simple as possible, neglect for now the pressure change across the meniscus due to surface tension so that $P_3 = P_\infty$. Combining the previous two expressions results in an ordinary differential equation which, for $U_o(0) = 0$, may be solved to yield

$$\frac{U_o}{U^*} = \tanh\left[\frac{U^* t}{2\,(2h + L_o)}\right] \tag{2.9}$$

where

$$U^* = \sqrt{\frac{2jBL_o}{\rho}} \tag{2.10}$$

is the maximum achievable velocity.

The Weber number and ejected volume are easily calculated using Equation 2.9. Imposing the volumetric constraint

$$V_{eject} = 1 \ drop \ volume = \frac{1}{6}\pi h^3 \tag{2.11}$$

leads to the following expression for the Weber number evaluated at $t = t^*$, We_{crit}:

$$We_{crit} = \frac{(jL_o h)B}{\sigma} f\left(\frac{L_o}{h}\right) \tag{2.12}$$

The function $f(L_o/h)$ may be written as

$$f\left(\frac{L_o}{h}\right) = \tanh^2\left\{\operatorname{arccosh}\left[\exp\left(\frac{\pi/12}{L_o/h + 2}\right)\right]\right\} \sim \frac{\pi/6}{L_o/h + 2} \tag{2.13}$$

where the simplified form results from the assumption that $U^* >> U_o$. Recognizing that the product jL_oh is the current, I, passed through the conductor gives

$$IB = \frac{We_{crit}\sigma}{f(L_o/h)} \tag{2.14}$$

For a typical solder ejection with $L_o/h = 2$ and $We_{crit} = 20$, the product IB must at least exceed 80 N/m (1 N/m = 1 AT) in order to successfully eject a droplet of diameter h. A pair of high quality off-the-shelf permanent magnets generate a magnetic field of just

under 2 T, [Edmund Scientific 1995] so a current of order 40 A needs to be sustained for about 10 μs to use MHD to dispense the solder droplet.

This analysis helps to illustrate some of the tough technical problems associated with the MHD design, but also reveals a very interesting detail that could prove important as manufacturers seek methods for producing even smaller diameter droplets. The critical Weber number as defined in Equation 2.12 is only dependent on the ratio L_o/h; it is independent of the actual dimensions of these features. As long as the current density does not exceed levels which cause catastrophic electromigration in the conductive leads, this design can be scaled to smaller and smaller dimensions.

2.3.2 Piezoelectric System

The piezoelectric materials considered for this application are brittle ceramic solids silvered on two sides to form what resembles a flat plate capacitor with a dielectric insert. Their primary uses derive from their electromechanical coupling: when a electric field is applied, a mechanical strain is generated in the ceramic, and when a mechanical stress is applied an electric field is established between the conductive faces. As shown in the conceptual piezoelectric system pictured earlier, the actuator compresses the volume of fluid just upstream of the orifice, and the resulting pressure drives the fluid outward.

Piezoelectric drop-on-demand systems are currently used in many commercial ink jet and wax printers. Although much of the technical analysis performed on these models involves proprietary methods, a significant literature database exists which describes many experimental devices. [Shield *et al* 1987, Kyser *et al* 1981, Stemme and Larsson 1972] The piezoelectric design is intrinsically more flexible than an MHD design for several reasons. First of all, both non-conductive and conductive fluids are acceptable in many designs. With a relatively small rework effort, the critical components of the piezoelectric system may be interchanged, adjusted, or otherwise modified to produce dramatic changes in system performance. The most significant disadvantage is that the performance of the piezoelectric actuator degrades dramatically when its temperature exceeds roughly one-

half of the Curie Point of the material. With high quality piezoelectric materials this constraint limits operation to peak temperatures below 230°C, [Stacy 1993] so eutectic solder (T_{melt} = 183°C) is still feasible, but higher melting point materials will require actuator cooling.

A brief scaling analysis helps to form a preliminary assessment of the feasibility of using a piezoelectric system for solder ejection. Assuming a constant driving pressure the approximate momentum equation from Equation 2.6 is readily integrated to show that

$$U_o = \frac{P}{\rho L_o} t \tag{2.15}$$

With this expression, it is straightforward to calculate the Weber number and the flow rate as functions of time. As in the previous section, imposing the V_{eject} = 1 drop volume constraint leads to an expression for the critical Weber number which becomes

$$We_{crit} = \frac{8}{3} \frac{P}{\sigma/a_o} \frac{a_o}{L_o} \tag{2.16}$$

Assuming that an infinitely rigid piezoelectric actuator uniformly compresses the circular end of a closed cylindrical chamber of fluid of height L_c by a small distance x, thermodynamic arguments predict that the resulting fluid gage pressure is

$$P = \frac{1}{\kappa_s} \frac{x}{L_c} \tag{2.17}$$

where κ_s is the isentropic compressibility of the fluid. Combining and rearranging Equations 2.16 and 2.17 eventually gives the desired expression

$$x = \frac{3}{8} We_{crit} \left(\frac{L_o}{a_o}\right) \left(\frac{\sigma}{a_o} \kappa_s\right) L_c \tag{2.18}$$

For solder ejection with We_{crit} = 20, effective L_o = 225 μm, a_o = 25 μm, and L_c = 500 μm, an actuator displacement of order 20 nm is required. Depending upon the actuator configuration and the applied voltage, a standard piezoelectric driver may provide displacements up to two orders of magnitude larger than this calculated value.

These preliminary calculations suggest that the piezoelectric design concept is more viable than the magnetohydrodynamic one. The calculations, along with the commercial use of piezoelectric designs, led to the belief that solder dispensing could be quickly and easily achieved using this technology. The new drop-on-demand system would require a from-the-ground-up redesign which would account for the physical properties of molten solder and use a high Curie temperature piezoelectric actuator.

CHAPTER 3

Modelling Droplet Ejection

3.1 Background

After the construction and unsuccessful operation of several mock-ups of the piezoelectric concept, it became clear that a more refined theoretical model of the pressurization and ejection process was required. This Chapter presents this modelling effort, and describes the procedure used to solve the governing equations for the drop-on-demand device. "Optimum" design conditions are presented, and the effect of parameter variation from this reference point on overall performance is discussed.

To rapidly and efficiently explore a wide range of design possibilities for a given working fluid, a drop-on-demand designer should have the ability to study the performance of a proposed configuration long before manufacturing commences. The evaluation flow chart for analyzing a drop-on-demand system is shown in Figure 3.1. To obtain a successful theoretical design, it is necessary to develop governing equations for the device, and to adopt a systematic method for modifying the input parameters to achieve a desired change in output.

Figure 3.2 shows a cross section of the drop-on-demand system analyzed in this Chapter. The co-fired bundle of piezoelectric drivers shown on the left side of this diagram pushes against a piston which deflects a thin metal diaphragm covering the compression chamber. The pressure of the working fluid rises in response to this motion, and forces fluid out through the orifice and back toward the reservoir through the restrictor channel. After the termination of the voltage signal and the snap-off of the droplet, fluid from the reservoir replenishes the depleted orifice channel under the action of capillary and possibly hydrostatic forces.

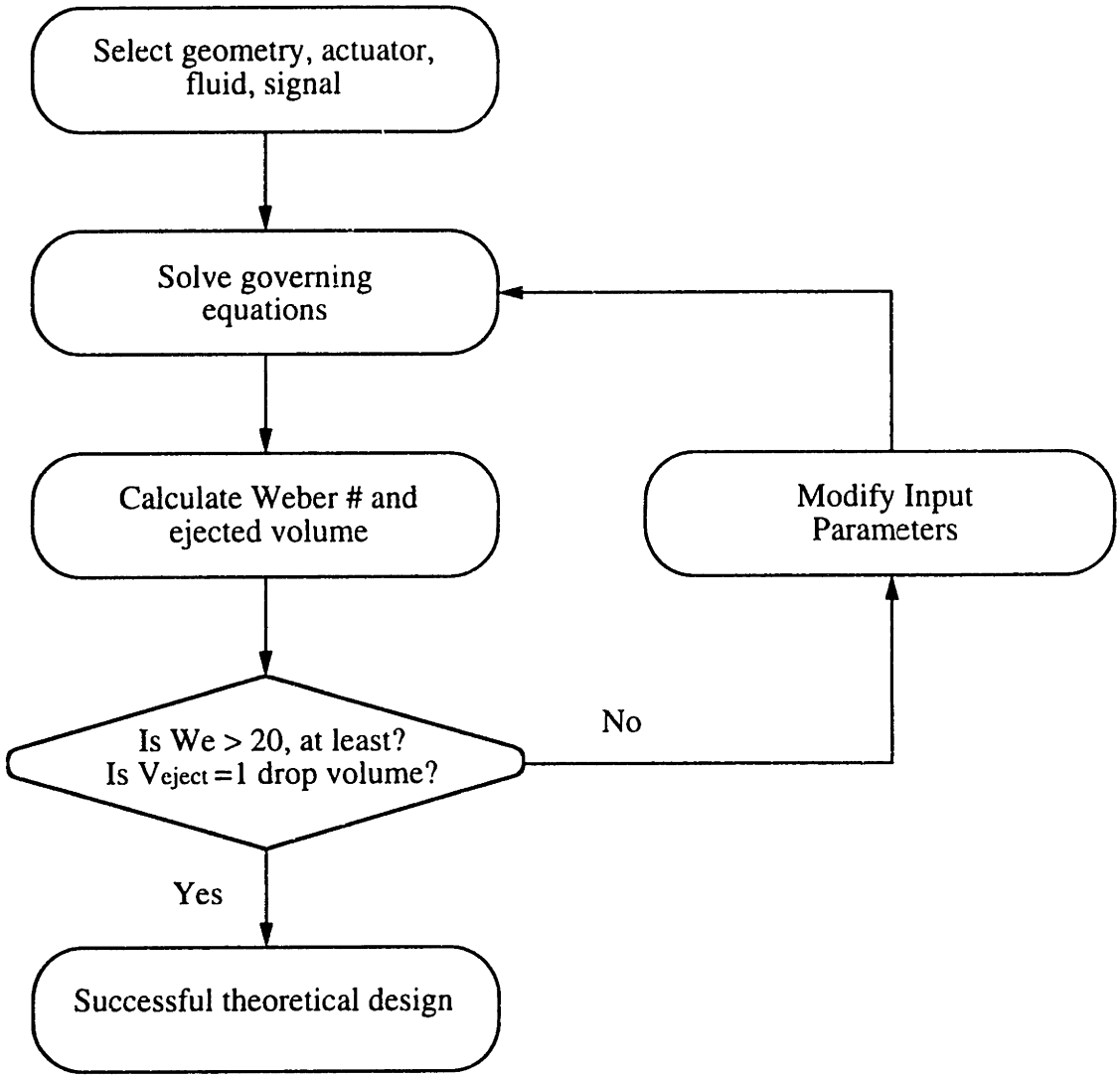

FIGURE 3.1 Design evaluation flow chart

3.2 Analysis of the Piezoelectric Actuator

In order to best explain their operation, it is instructive to briefly discuss the piezoelectric phenomenon in terms of the crystalline structure of the materials. Most simply put, "Piezoelectricity is the phenomenon in which certain crystalline substances develop an electric field when subjected to pressure forces, or conversely, exhibit a mechanical deformation when subjected to an electric field." [Piezo Kinetics Incorporated

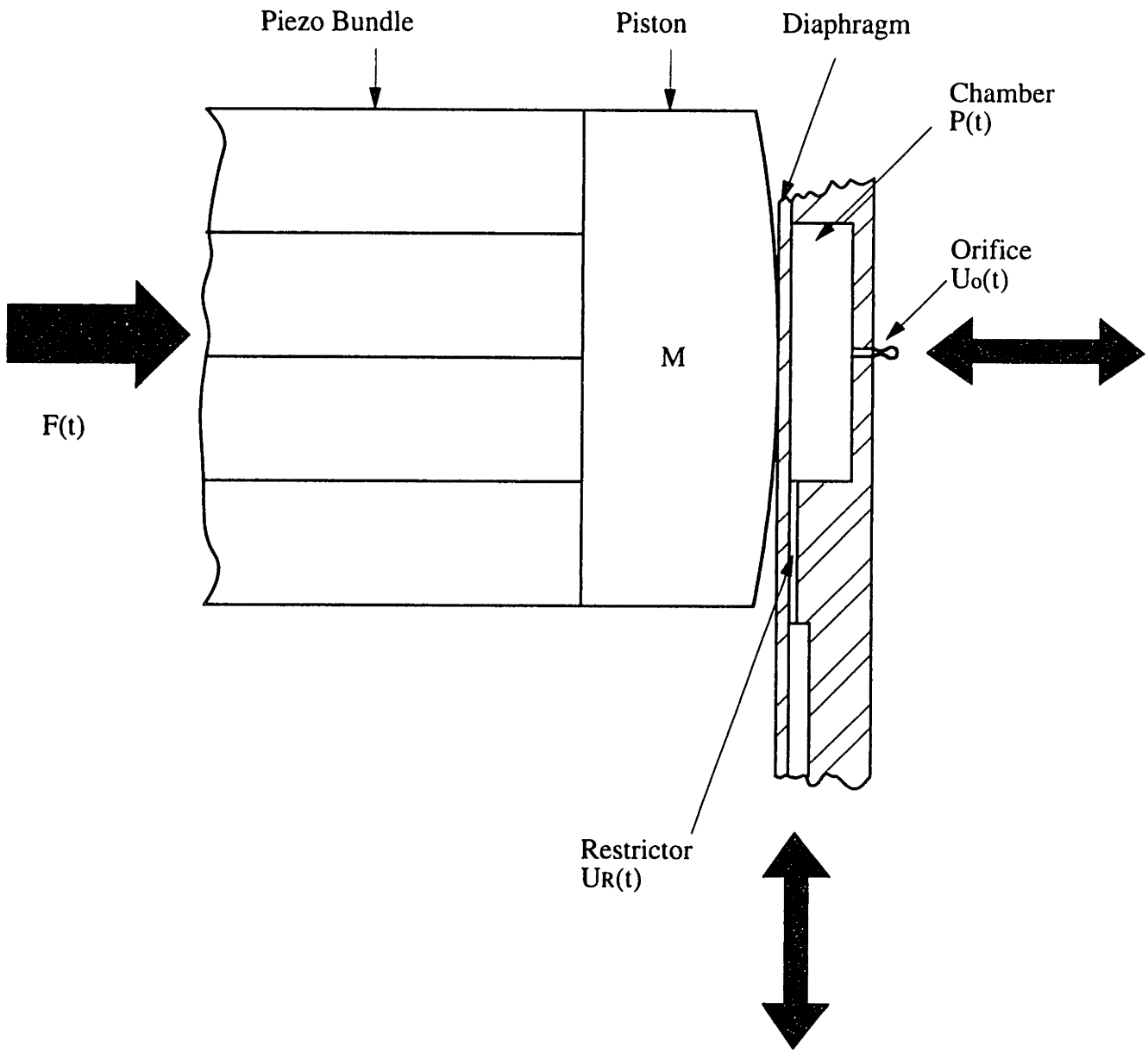

FIGURE 3.2 Cross sectional view of the critical components of the drop-on-demand system

1993] The effect is only found in materials such as quartz, Rochelle salt, and several synthetic substances which exhibit no crystalline center of symmetry,

The piezoelectric materials used in this research effort are composed of lead zirconate titanate. To instill piezoelectric properties in synthetic substances requires special processing. First, the material is fashioned into the desired geometry, and the metallic electrodes are applied. The piece is then heated to a temperature above the Curie point of the substance in the presence of a strong DC electric field. "This polarizes, or poles, the ceramic (aligns the molecular dipoles of the ceramic in the direction of the applied field) and provides it with its piezoelectric properties."

A linearized constitutive theory presents a unified model for the electromechanical behavior of the piezoelectric materials. The Cartesian constitutive relations are written in tensor form as [Bugdayci *et al* 1983]

$$\begin{aligned} \varepsilon_{ij} &= s_{ijkl}\,\sigma_{kl} + g_{kij}\,D_k \\ E_i &= -g_{ikl}\,\sigma_{kl} + \beta_{ij}\,D_j \end{aligned} \tag{3.1}$$

The strain tensor, ε_{ij}, depends upon the product of the material compliance, s_{ijkl}, and the stress tensor σ_{kl}, as well as on the product of the voltage coefficient, g_{kij}, and the electric displacement vector, D_k. The electric field vector, E_i, depends upon the applied mechanical stress and the dielectric coefficient, β_{ij}. Bugdayci explains that when all the equations needed to completely describe the piezoelectric are counted, not fewer than "...22 field equations in 22 variables that are functions of time t and position (x_1, x_2, x_3)" are required.

The piezoelectric equations reduce to extremely simple formulations under certain simplifying conditions. For instance, if the piezoelectric is not driven near a resonant frequency, it is often convenient to assume that the applied signal and resulting motion are approximately quasi-static. The resulting governing equations may then be classified into two basic categories: "motor" relations in which the piezoelectric acts as an actuator, and "generator" equations in which the ceramic acts as a transducer. In the proposed

drop-on-demand system, the piezoelectric simultaneously functions as both a motor and as a generator. Referring to Figure 3.3 and Table 3.1, the governing equation for N drivers bundled together is

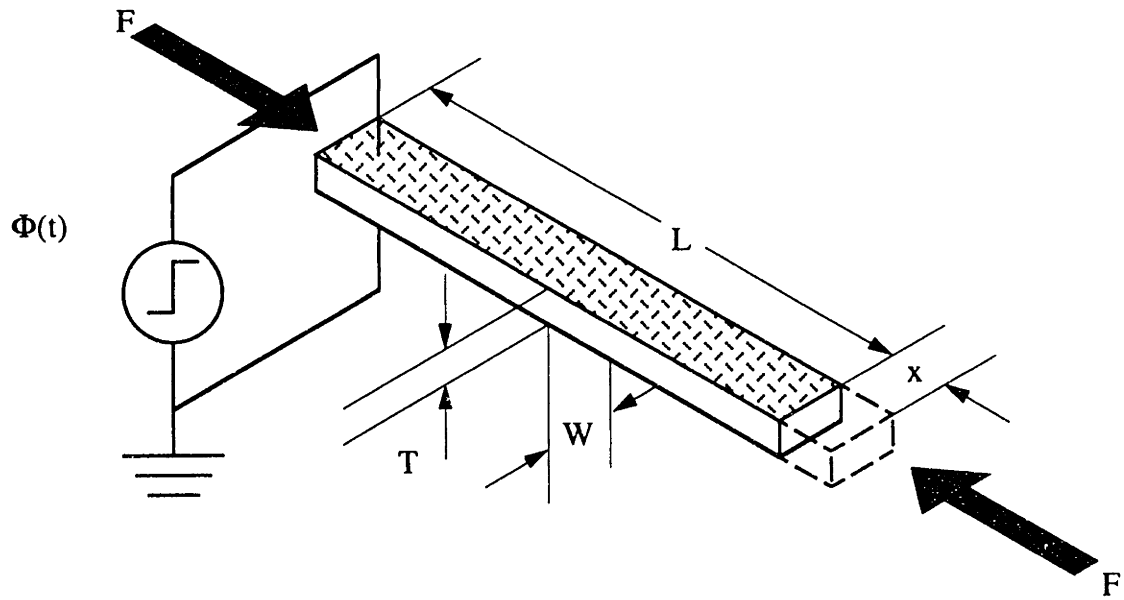

FIGURE 3.3 The piezoelectric plate acts as a "motor" and as a "generator"

L *(mm)*	38.1
W *(mm)*	2.0
T *(mm)*	.5
$d_{31}x10^{10}$ *(m/V)*	1.75
$s_{11}^{E}x10^{10}$ *(m/N)*	.16

TABLE 3.1 Data for a single piezoelectric plate used in the second prototype. Values reflect the properties of APC 850 material ceramic. [American Piezo Ceramics 1992]

$$\frac{x}{L} = \left(\frac{\Phi}{T}\right) d_{31} - \left(\frac{F}{NTW}\right) s_{11}^{E} \tag{3.2}$$

where x, L, T, and W correspond to the dimensions shown in the Figure, Φ and F are the applied voltage and compressive force, and d_{31} and s_{11}^{E} are piezoelectric constants. The equation may be compactly written as

$$x = \alpha \Phi - \beta F \tag{3.3}$$

where α and β are constants as dictated by Equation 3.2.

Analytic solution even to the simplified equations can become nearly intractable when the geometry or boundary conditions are not simple. The analysis of the bilaminar plate actuator described in Chapter 5, for instance, requires an interfacial boundary condition and properties and geometries for two different materials. An approximate solution for this case is given in the literature. [Stemme and Larson 1972]

3.3 Modelling of the Compression Chamber

The next step in the development of the governing equations for the drop-on-demand system is the application of Newton's Second Law to the piston. This small metallic "button" is accelerated by the force generated by the piezoelectric bundle, and is decelerated by the stiffness of the diaphragm and the pressure in the chamber. The pressure is assumed uniform throughout the chamber volume because the acoustic time scale associated with this pressure rise is at least one order of magnitude smaller than other time scales in this problem. Referring to Figure 3.4, Newton's Second Law is immediately written as

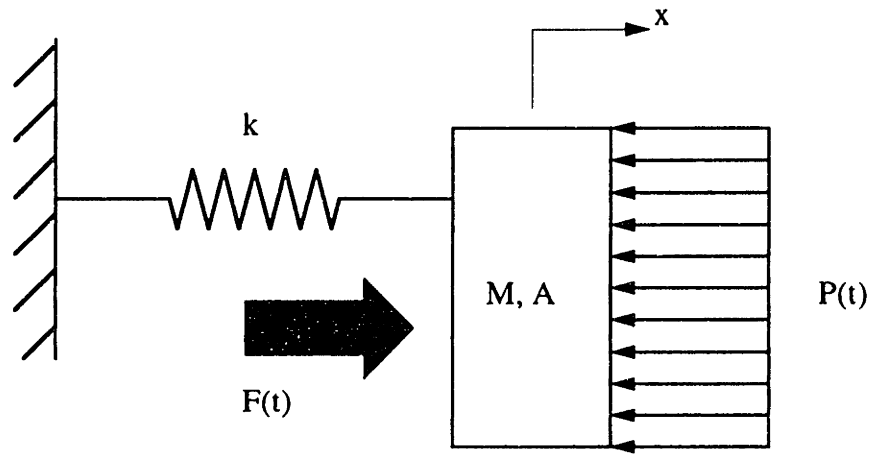

FIGURE 3.4 Model of the mass-spring system which approximates the actuator-chamber relationship

$$M \frac{d^2x}{dt^2} = F(t) - P(t)A - kx \tag{3.4}$$

When the piezoelectric equation from Section 3.2 is introduced, the expression may be recast as

$$M \frac{d^2x}{dt^2} + \left(k + \frac{1}{\beta}\right) x = \frac{\alpha}{\beta} \Phi - PA \tag{3.5}$$

This segment of the device behaves as a mass-spring system driven by a forcing function composed of terms involving the applied voltage signal and the chamber pressure.

The input electronic signal is chosen by the designer, but the chamber pressure is a dependent quantity. To determine this still unknown variable, consider the control

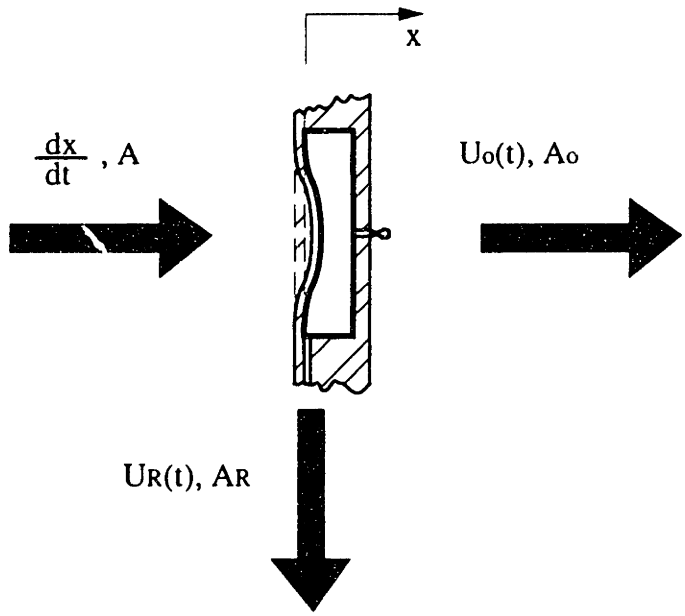

FIGURE 3.5 The control volume inside of the chamber is highlighted by the bold line.

volume highlighted with the bold line in Figure 3.5. Applying the conservation of mass to the drop-on-demand chamber shows that

$$\frac{d}{dt}(\rho V) + \rho_i U_o A_o + \rho_i U_R A_R = 0 \tag{3.6}$$

Here V is the volume of the control volume and the subscripts "o" and "R" refer to the orifice and restrictor, respectively. The subscript "i" indicates the initial value of the value of the variable, and A denotes cross sectional area. The derivative in this relationship is expanded and linearized to account for small changes is density and volume so that

$$\frac{d}{dt}(\rho V) \sim V_i \frac{d\rho}{dt} + \rho_i \frac{dV}{dt} \tag{3.7}$$

Recognizing that the rate of change of volume is related to the piston velocity, dx/dt, and that the rate of change of density may be estimated using thermodynamic theory shows that

$$\frac{dV}{dt} = -\gamma A \frac{dx}{dt}$$

$$\frac{d\rho}{dt} = \rho \kappa_s \frac{dP}{dt} \tag{3.8}$$

In Equation 3.8 γ is a constant (approximately one third) which accounts for the curvature of the diaphragm, and κ_s is the isentropic compressibility of the fluid[&]. Rearrangement finally gives the desired differential equation for the time rate of change of pressure

$$\frac{dP}{dt} = \frac{1}{\kappa_s V_i}\left(\gamma A \frac{dx}{dt} - U_o A_o - U_R A_R\right) \tag{3.9}$$

Note that when the piston velocity term is much larger than the outflow terms, the pressure depends directly upon the piston displacement x, which oscillates according to Equation 3.3. In the optimized design, the outflow terms do slightly influence the chamber pressure, and cause a gradual roll-off in the magnitude of this quantity. In other off-optimum designs the decay can be much more pronounced.

[&] The process was considered isentropic instead of isothermal because the compression time scale is much smaller than the heat transfer time scale. The chamber essentially acts as an adiabatic vessel, and the compression stroke is assumed reversible. The isentropic/isothermal compressibility decision is not critical because the properties are roughly equal for liquids.

3.4 Determination of the Fluid Velocity

An analysis of a drop-on-demand system requires relationships describing the transient velocity history of the fluid in the orifice and the restrictor. To model these flows, consider the diagram shown in Figure 3.6. Since the density changes in the liquid flowing along the streamlines are small, assume that this property is constant. Consider also the velocity profile of a Newtonian fluid with kinematic viscosity η which flows through this small orifice. The length of this through hole is typically no more than two or three times its diameter, and the time scale for the flow is of the order of tens of microseconds. For fluids with viscosities of the order of that of water or solder, the flow will not attain a fully-developed, parabolic profile because the boundary layer thickness, δ, inside of the channel is always significantly smaller than the characteristic geometric dimensions. The same argument applies for the restrictor as well, so that in general

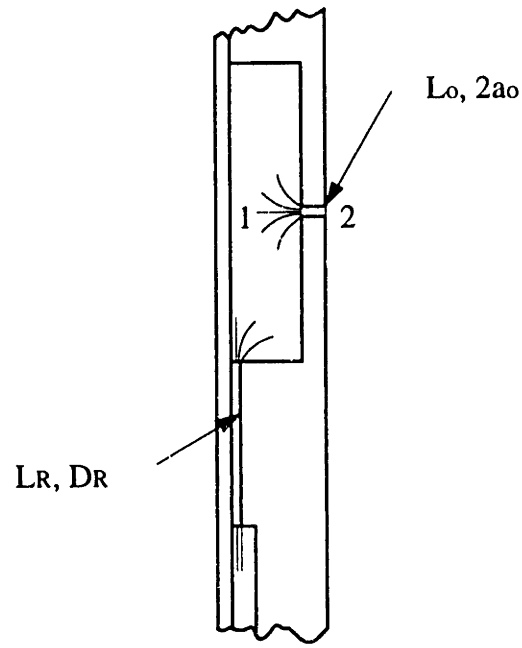

FIGURE 3.6 Pressurization causes outflow from the chamber along the streamlines shown here.

$$\delta \sim \sqrt{\eta \tau} < a_o, \frac{D_R}{2} \tag{3.10}$$

where τ is the characteristic time for flow direction reversal. Further discussion of this time scale appears in Section 3.6.

The constant-density, inviscid, unsteady flow along a streamline may be modelled using the unsteady Bernoulli equation,

$$\int_1^2 \frac{\partial U}{\partial t} ds + \left(\frac{P}{\rho} + \frac{1}{2} U^2 + gz \right)_2 - \left(\frac{P}{\rho} + \frac{1}{2} U^2 + gz \right)_1 = 0 \qquad (3.11)$$

For the flow of fluid in the orifice, assume that $U_1 << U_2$ because of the disparate areas of the chamber and orifice, and that the hydrostatic terms are small compared to the other terms in the relation. The pressure at point 1 is the chamber pressure, P, and the pressure at point 2 is the gage pressure just inside of the meniscus. To a first approximation the pressure rise due to surface tension at point 2 may be neglected, so that $P_2 \approx 0$. The numerical procedure which follows uses a slightly more accurate representation, where this pressure is approximated as a piecewise continuous linear function of meniscus position. Kyser derived an explicit, non-linear form for this pressure term for this geometry. [Kyser *et al* 1981]

The integral term in the unsteady Bernoulli equation requires some special attention, because the acceleration of the fluid is not constant along the streamline stretching from 1 to 2. Continuity arguments show that there is a region near the orifice entrance in which the fluid acceleration increases from its value at point 1 to the comparatively high value in the orifice channel. To account for the acceleration of this entrance region fluid during ejection, two hydraulic diameters were added to the effective length of the orifice. This is by no means exact, but represents a fair and simple approximation. In terms of the system variables the unsteady Bernoulli equation becomes

$$\frac{dU_o}{dt} = \frac{1}{L_o + 4a_o} \left(\frac{P}{\rho} - \frac{1}{2} U_o^2 \right) \qquad U_o > 0 \qquad (3.12)$$

for $P_2 << P_1$. Similarly, for ejection from a restrictor of hydraulic diameter D_R, length L_R, and flow velocity U_R,

$$\frac{dU_R}{dt} = \frac{1}{L_R + 2D_R}\left(\frac{P}{\rho} - \frac{1}{2}U_R^2\right) \qquad U_R > 0 \qquad (3.13)$$

Equations 3.12 and 3.13 apply only for outflows from the chamber. For negative velocities, the streamlines at the orifice entrance do not contract in the same manner as shown in the Figure. This, and the difference in directions of these velocities, leads to the following alternate expressions for the inflow velocities:

$$\frac{dU_o}{dt} = \frac{P}{\rho L_o} \qquad U_o < 0$$

$$\frac{dU_R}{dt} = \frac{1}{L_R + 2D_R}\left(\frac{P}{\rho} + \frac{1}{2}U_R^2\right) \qquad U_R < 0 \qquad (3.14)$$

Since capillary forces draw fluid into the orifice from the reservoir during the refill phase, the surface tension terms must be included in the velocity relations to properly model this stage. The mathematical model of the piezoelectric drop-on-demand system is now represented by Equations 3.5, 3.9, 3.12, 3.13, and 3.14.

3.5 Droplet Snap-Off and Flight

The theoretical analysis of the fluid which speeds from the orifice involves surface tension, viscous, and inertial terms. Researchers have attempted to numerically simulate the ejection phenomenon with some success [Fromm 1984, Wallace 1989], but this level of detail is not necessary for our purposes. A much simpler scheme was suggested by Kyser *et al*, [1981] who divided the ejection process into four distinct phases:

1. Chamber pressure is positive. Fluid in the orifice is accelerating outward.
2. Chamber pressure is negative. Fluid in the orifice is decelerated, but still has positive velocity.
3. Chamber pressure is negative. Fluid velocity in the orifice has become negative. Droplet detaches.
4. Surface tension forces refill the orifice to replace ejected fluid. Pressure relaxes to equilibrium.

Throughout this present work, the model was simplified by assuming that the droplet detaches from the connecting fluid tail after the electronic driving signal returns to its ground state of zero volts. This snap-off time estimate places droplet break-off in between phases 2 and 3 in the Kyser scheme, and therefore conservatively underestimates the volume of the resulting droplet. Even though the droplet is decelerated slightly by the action of the surface tension forces which act in the tail region, and by the inertia of the droplet itself, the snap-off velocity was taken to be the maximum meniscus velocity attained during the pressure pulse. More precise attempts to model the details of the ejection should include these effects.

Although not directly relevant to the design of the droplet dispenser, it is instructive to consider the trajectory of the droplet as it flies in a viscous, gaseous environment after ejection. This calculation helps ensure that the droplets arrive at the target with sufficient speed to assure ballistic accuracy. The analysis is fairly straight forward using the drag coefficient estimates [Bird *et al* 1960; Probstein and Fassio 1970]

$$\begin{aligned} C_D &= 24\ Re^{-1} && Re < 1 \\ C_D &= 24\ Re^{-3/5} && 1 < Re < 10^3 \end{aligned} \qquad \textbf{(3.15)}$$

Rearrangement of the integrated one dimensional equation of motion for a droplet of radius a and density ρ shows that [Gao 1994]

$$\frac{l_s}{a} = \begin{cases} \dfrac{5}{27}\dfrac{\rho}{\rho_g}\left[\left(\dfrac{\rho_g U_o\, 2a}{\mu_g}\right)^{3/5} - \dfrac{2}{5}\right] & 1 < Re_o < 10^3 \\ \dfrac{1}{9}\dfrac{\rho U_o\, 2a}{\mu_g} & Re_o < 1 \end{cases} \qquad \textbf{(3.16)}$$

In the expressions, l_s refers to the distance travelled before the droplet velocity reaches zero (the stopping distance), μ corresponds to the absolute viscosity, and the Reynolds

number is $Re = \rho_g U(2a)/\mu_g$. The subscripts "g" and "o" refer to the gaseous environment and the orifice exit, respectively. Since the stopping distance is an easily measured quantity, Equation 3.16 proves especially useful in producing an estimate of the ejection velocity.

3.6 Numerical Solution of Governing Equations

The ordinary, non-linear differential equations which describe the system model of the drop-on-demand device can, in principle, be solved with the appropriate initial conditions to determine the liquid's displacement, velocity, acceleration, pressure, volume flow, and Weber number as functions of time. Since an analytical solution could only be found when terms of significance were neglected, a numerical solution technique was employed to solve the governing equations. A constant size time step which was at least one-fifth, and usually one-tenth, the duration of the rise time of the applied voltage pulse was used. The transient variables were updated by using the following relations, which are based upon the governing equations:

$$\left(\frac{dx}{dt}\right)_{i+1} = \frac{1}{M}\left[-\left(k + \frac{1}{\beta}\right)x + \frac{\alpha}{\beta}\Phi - PA\right]_i \Delta t + \left(\frac{dx}{dt}\right)_i \qquad (3.17)$$

$$(P)_{i+1} = \frac{1}{\kappa_s V_o}\left[\gamma A\left(\frac{dx}{dt}\right)_{i+1} - (U_o)_i A_o - (U_R)_i A_R\right]\Delta t + (P)_i \qquad (3.18)$$

$$(U_o)_{i+1} = \frac{1}{L_o + 4a_o}\left[\frac{(P)_{i+1}}{\rho} - \frac{1}{2}(U_o)_i^2\right]\Delta t + (U_o)_i \qquad (3.19)$$

$$for\ U_o > 0$$

$$(U_o)_{i+1} = \frac{1}{L_o}\left[\frac{(P)_{i+1}}{\rho}\right]\Delta t + (U_o)_i \qquad (3.20)$$

$$for\ U_o < 0$$

$$(U_R)_{i+1} = \frac{1}{L_R + 2D_R}\left[\frac{(P)_{i+1}}{\rho} - \frac{1}{2}(U_R)_i^2\right]\Delta t + (U_R)_i \qquad (3.21)$$

$$for\ U_R > 0$$

$$(U_R)_{i+1} = \frac{1}{L_R + 2D_R}\left[\frac{(P)_{i+1}}{\rho} + \frac{1}{2}(U_R)_i^2\right]\Delta t + (U_R)_i \qquad (3.22)$$

$$for\ U_R < 0$$

In each of these relationships the subscript "i" denotes the current time step, and "i+1" denotes the next time step.

This numerical scheme makes it simple to add further detail to the drop-on-demand model. For instance, assuming a fully developed, viscous flow in the restrictor channel helps to illustrate the qualitative effects of fluid viscosity on overall system performance. These head losses may be directly included in the unsteady Bernoulli analysis. The model may also be modified to include the effects of the hydrostatic

pressure which results from reservoir elevation. The dynamic dependence of contact angle on meniscus velocity could be included in the numerical model by introducing the empirical relation [Hoffman 1975]

$$\theta_d^3 = \frac{\mu U}{\sigma} \frac{1}{\kappa} + \theta_o^3 \qquad (3.23)$$

where the non-dimensional group $\mu U/\sigma$ is the Capillary number, the constant κ is approximately 1.3 x 10^{-2} rad^{-3}, and θ_o and θ_d are the static and dynamic contact angles, respectively.

Figure 3.7 shows the computed response of the system variables to a trapezoidal voltage pulse. The values of the design parameters and summary statistics for the simulation are shown in Table 3.2. The frequency of oscillations in the pressure and velocity functions correspond to the natural frequency of the mass-spring system described in Section 3.3. The slight roll-off in the peak pressure value during this cycling occurs because fluid is ejected from the chamber during the elapsed time in between the peaks.

The velocity histories in the orifice and restrictor reveal an important feature of the drop-on-demand system: the ducts are sized so that the restrictor acts as an inertial check valve during the compression stroke. For short times after the application of the signal, the fluid in the orifice accelerates rapidly and ejects from the exit. The fluid in the restrictor accelerates more slowly because of the longer length of this channel. During the typical ejection roughly equal volumes of fluid (1.0 compared to 1.3 drop volumes) pass through the orifice and restrictor during the typical compression stroke. If too much fluid "leaks" through the restrictor during compression, the peak pressure value will decay rapidly and orifice velocity will be reduced accordingly.

Over longer time scales, the restrictor allows for replenishment of the fluid ejected from the orifice. This refill process is largely controlled by the retraction of the piezoelectric bundle and capillary action in the orifice, and is slightly affected by the hydrostatic pressure created by the positioning of the reservoir with respect to the orifice.

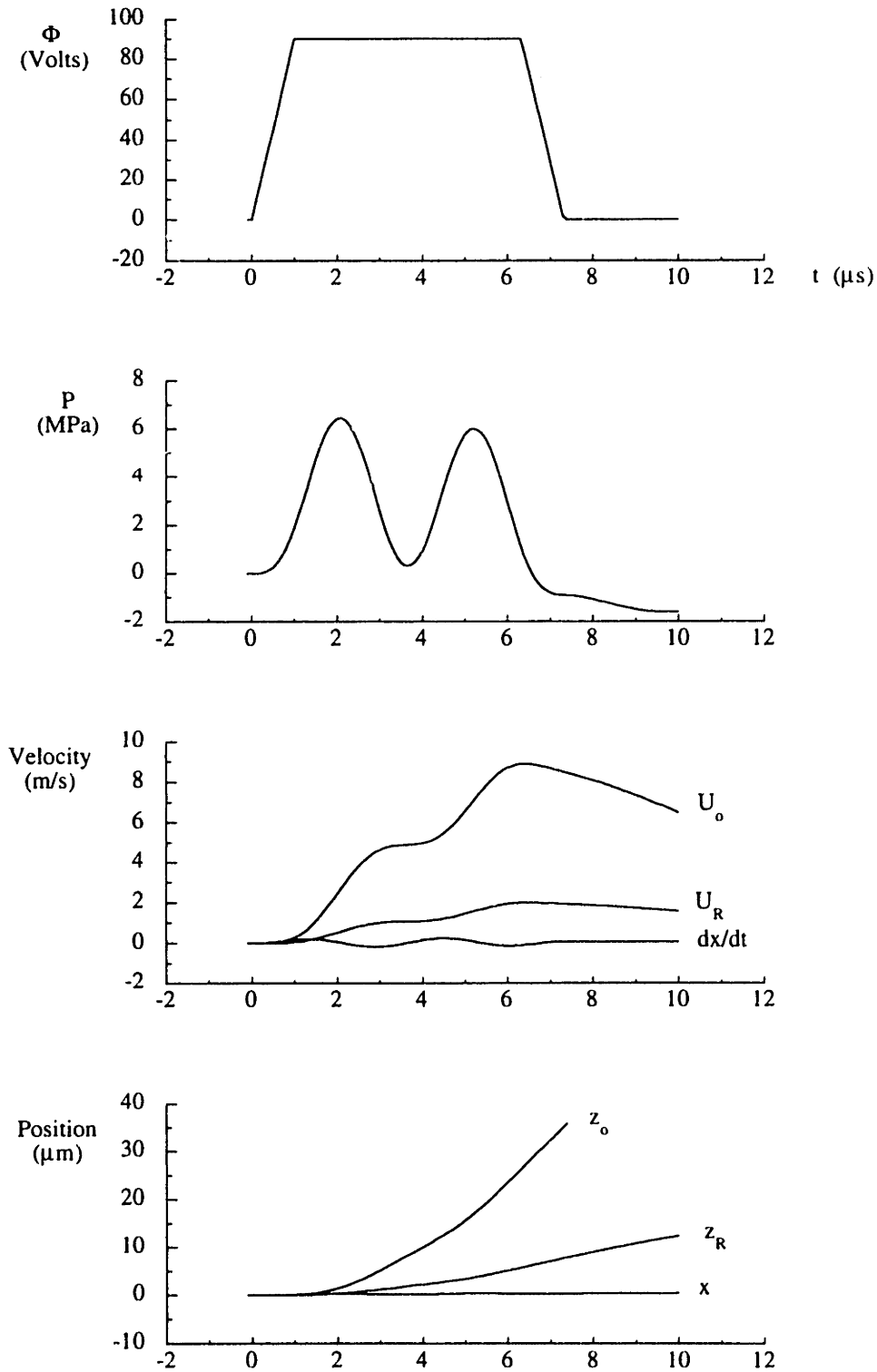

FIGURE 3.7 Input of a trapezoidal signal $\Phi(t)$ causes pressure P(t), piston velocity dx(t)/dt, orifice and restrictor outflow velocities $U_o(t)$ and $U_R(t)$, and corresponding displacements x(t), $z_o(t)$, and $z_R(t)$.

Design Parameters:	
α *(μm/V)*	1.33×10^{-2}
β *(μm/N)*	0.15
ρ *(kg/m³)*	9400
σ *(N/m)*	0.50
A *(mm²)*	1.96
A_o *(mm²)*	2.2×10^{-3}
A_R *(mm²)*	1.3×10^{-2}
c *(m/s)*	2060
k *(N/μm)*	.47
L_c *(μm)*	370
L_o *(μm)*	130
M *(μg)*	17
The applied signal:	
Pulse Width *(μs)*	5.3
Rise/Fall Time *(μs)*	1.0
Δt *(μs)*	.1
Φ *(V)*	90
For the ejected droplet:	
U_o *(m/s)*	8.9
V_{eject} *(drops)*	1.0
We	40
During the actuation:	
x_{max} *(μm)*	.36
P_{max} *(MPa)*	6.4

TABLE 3.2 Important parameters and summary statistics for a typical ejection

Since the inertia of the chamber fluid is not included in the model of the retraction of the diaphragm, the numerical results pertaining to the refill are regarded with due caution. However, it is conservative to assume that the characteristic time scale for flow direction reversal is roughly twice the pulse width. This approximation is supported by the inexact refill model, and with the help of Equation 3.11, shows that the inviscid assumption is an acceptable one.

3.7 Sensitivity to Design Parameters

The governing equations for the drop-on-demand system reveal important parameter sensitivities and couplings. Although every parameter included in these relations serves an important purpose, several of them take on particularly critical roles in determining the success or failure of solder ejection. To illustrate this, numerical simulations were carried out at a fixed reference point. Parameters were then individually varied and the values of important ejection variables were compared to the test case.

One of the most influential parameters is the radius of the pressure chamber. It appears in the mass-spring and pressure differential equations through the chamber area A and the chamber initial volume V_i. These equations suggest that a decrease in chamber area will increase the peak pressure value, but if the area becomes too small, the peak pressure roll-off will become disastrously rapid. Carrying out the simulation using a chamber radius just 0.15 mm smaller than the reference value (about a 19% reduction) causes the ejected volume to increase from 1.0 to 1.3 drop volumes and the ejection Weber number to increase from 40 to 85. This "improved" design is deceptive, for when the input signal is adjusted so that only 1.0 drop volumes eject from the orifice, the corresponding Weber number falls to 25. Increasing the radius of the chamber by this same increment results in 0.8 drop volumes of material being ejected with a Weber number of 24. Imposing the 1.0 drop volume ejected volume constraint requires a volatge signal of 150 V, which exceeds the 100 V capacity of our existing electronics hardware.

Similar arguments apply to the variations in the piezoelectric compliance β and

the length of the orifice channel L_o. Reducing β by increasing the number of piezoelectric actuators in the bundle should stiffen the driver, and hence improve the overall performance of the device. Doubling the number of actuators comprising the bundle increases the ejected volume from 1.0 to 1.7 drop volumes, and raises the ejection Weber number from 40 to 126. When the 1.0 drop volume constraint is imposed by adjusting the input signal, this alteration does increase the Weber number slightly above the reference value. The change was not implemented because of the significant temporal costs associated with assembling this marginally improved actuator.

The orifice acceleration equation suggests that a similar improvement may be obtained by reducing the length of the orifice duct. Numerically reducing this dimension by a factor of two raises the ejected volume from 1.0 to 1.3 drop volumes, and increases the Weber number from 40 to 80. However, the model suggests that to avoid the aspiration of air into the chamber after droplet ejection and subsequent meniscus retraction, the orifice should have a length of at least 125 μm.

The solutions to the governing differential equations suggest that solder dispensing is theoretically possible with this design, but the safety margin is not large. Remember that the above analysis functions as an inexact design tool which helps to explain the scaling laws of the drop-on-demand system. During the simulated ejection sequence detailed in Section 3.6, a sizable bundle of piezoelectric elements push out a single droplet of solder in response to a electrical pulse 90 V in magnitude. In light of the many assumptions and uncertainties in the model, this value was dangerously close to the 100 V limit on our pulse generator. Success or failure critically depends upon the accuracy of the simple model and the physical implementation of the resulting design.

CHAPTER 4

Subsystem Implementation and Experimental Setup

4.1 Overview

The devices constructed during this research effort followed an evolutionary process, with each new system addressing several new facets of the design problem. Extremely simple theoretical models were first used to develop mock-ups of the drop-on-demand system. Attempting to operate these devices helped to further our understanding of the scaling laws of the dispenser. After careful study of these devices and significant theoretical revision, two advanced prototypes of the system were designed and fabricated.

The prototypes of the droplet delivery system share a common layout. The reservoir feeds fluid into the device through a supply tube, which may be heated to allow for molten solder delivery. Once inside the base unit, the fluid travels into the chamber region, which consists of a diaphragm and chamber plate. In response to a voltage pulse, the piezoelectric actuator pushes the piston against the back side of the thin metal diaphragm which covers the chamber. The pressure of the working fluid increases in response to this motion, and a droplet ejects from the orifice. This Chapter focusses upon the practical design issues associated with the critical subsystems in the prototypes.

4.2 Piezoelectric Actuator

The assembly of the piezoelectric actuator required extraordinary care. The bilaminar plate used in the mock-ups was replaced with this co-fired array for two primary reasons. The first involved a geometric incompatibility: the smallest standard piezoelectric discs are about 5 mm in diameter, and the chamber is less than 2 mm in

diameter. It therefore proved difficult to rigidly clamp the perimeter of the fragile bilaminar plate. Secondly, firing multiple piezoelectric plates in parallel enhances actuator performance.

The assembly of the co-fired bundle is something of an art form. In the most recent of many iterations, four piezoelectric elements (each 38.10 mm ± .05 long, 1.94 mm ± .04 wide, and 0.53 mm ± .03 thick) were joined together using Epotech E-3084 (Epoxy Technology, Billerica, MA) high temperature, electrically conductive epoxy. (See Figure 4.1) Before assembly, the electrically conductive edges of the plates were bevelled with fine emery cloth to help reduce the risk of arcing during operation of the drop-on-demand device. Pairs of plates were fitted with tiny lead wires, epoxied together, and secured by a customized clamping fixture. Care was taken to prevent the oozing of epoxy from the sides of the bundle during the ensuing two hour, 190°C curing process, as this would cause an electrical short during operation. The bundle was annealed after curing to minimize thermal stress gradients. Finally, two pairs were joined into a foursome and the ends of the assembly were honed flat.

The first attempts at positioning and clamping the slender actuator relied upon the manual positioning of a lexan support fixture. This method required an extraordinary amount of human dexterity to avoid fracture of the actuator. In an attempt to improve this system, the feasibility of potting the bundle in electrically non-conducting epoxy was investigated. The method is viable, but was never successfully implemented. Attention was instead placed on the design and manufacture of a flexure based positioning system.

As shown in Figure 4.2, adjustment screws allowed actuator motion in the X and Y directions. The heat treated, spring steel flexures were designed so that the stiffnesses in the X and Y directions were comfortable to the user. A non-rotating micrometer head provided actuator adjustability in the Z direction. When the bundle was driven by an applied voltage signal and slowly advanced forward, an audible change in emitted frequency occurred upon contact with the diaphragm. After practicing at this technique, it was estimated that the rest position of the tip of the piston was repeatably placed less than .03 mm past the initial diaphragm contact point.

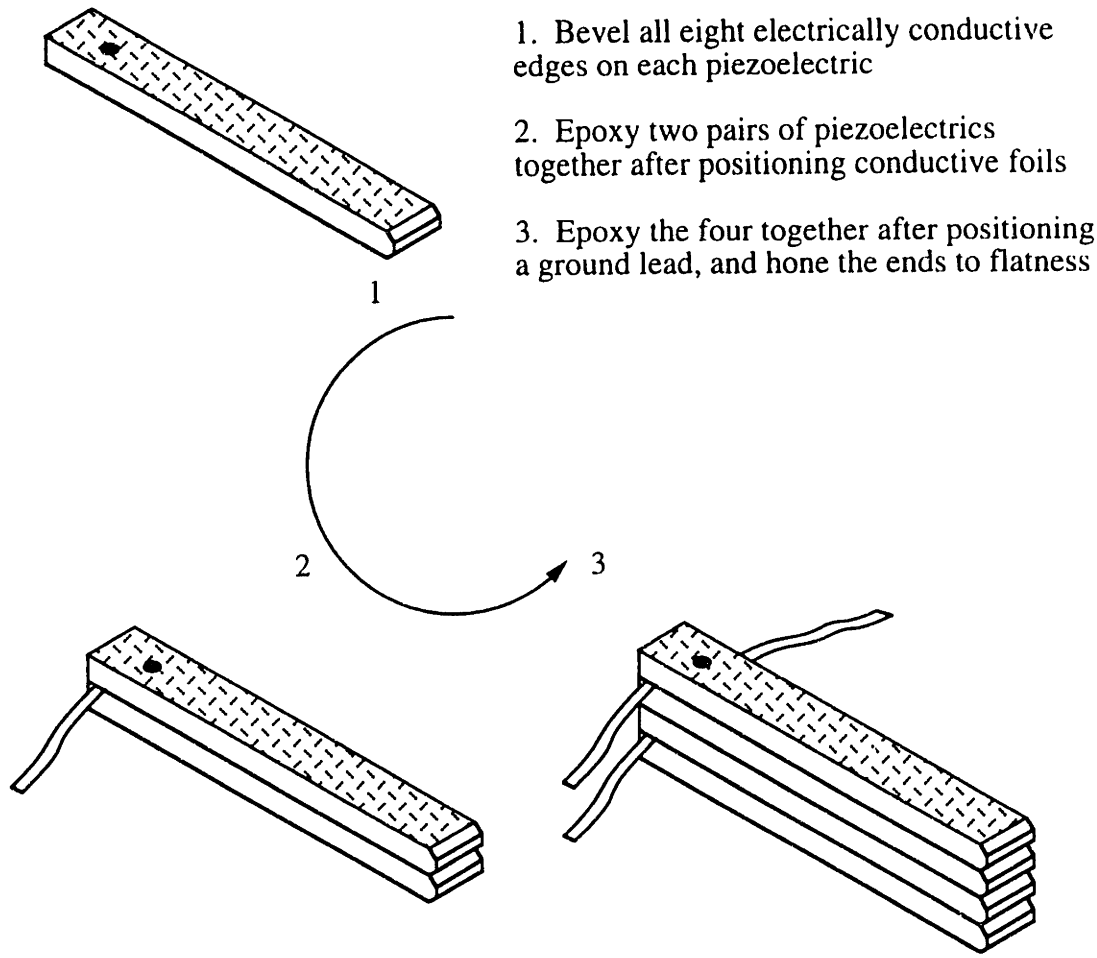

FIGURE 4.1 Assembly sequence for the co-fired piezoelectric bundle. Drawing not shown to scale.

4.3 Piston

The use of the high aspect ratio piezoelectrics was intended to eliminate the geometric mismatch between a relatively large diameter bilaminar plate and the tiny compression chamber. As our theoretical model evolved, it became clear that the successful ejection of liquid metal required that the bundle be significantly larger in cross sectional area than the chamber. The piston functions as the mechanical connection

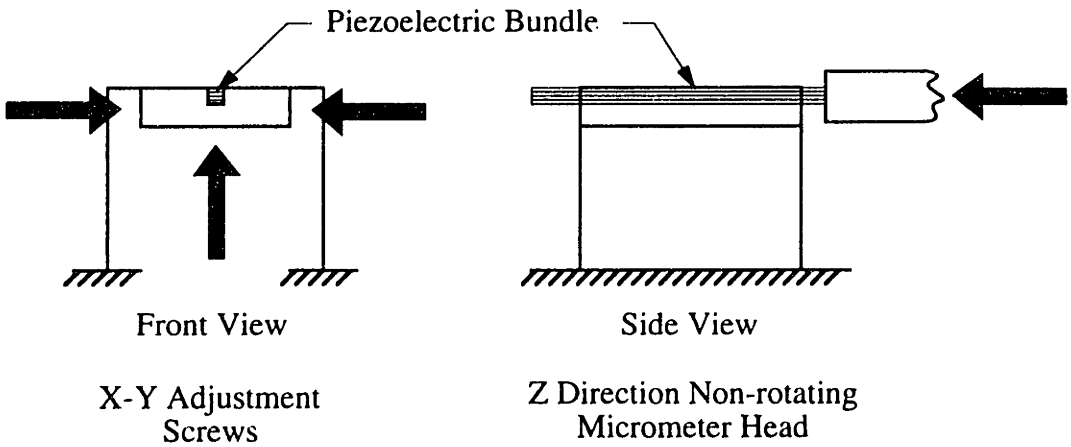

FIGURE 4.2 X-Y-Z adjustment system for the actuator

between these disproportionate components. In order to preserve the rapid submicron elongation of the driver, the piston must be light weight and stiff.

These requirements suggest that a material property optimization may help to improve the design of the piston. A back-of-the-envelope calculation showed that the period of the mass-spring system varies inversely with the ratio E/ρ^3. Thus, to minimize the piston response time, E/ρ^3 should be maximized. A selection of engineering materials are listed in Table 4.1, along with their relevant physical properties. The most optimal piston is composed of the expensive ceramic silicon carbide. The high electrical resistivity of alumina, sapphire, and ruby would help to prevent inadvertent shorting of the piezoelectric elements, but the materials are extremely difficult to machine. Graphite is easier to machine, but 6061 aluminum was selected because of its availability and machinability.

The preliminary analysis suggested that to provide adequate stiffness in bending,

	$Ex10^{-9}$ (N/m^2)	ρ (kg/m^3)	E/ρ^3	k_T (W/mK)	ρ_e $(\mu\Omega \cdot cm)$
Silicon Carbide	450[a]	3200[b]	18.5	84[b]	$1.5x10^{8}$ [d]
Alumina (Al_2O_3)	390[a]	3970[c]	6.6	36[c]	$1.0x10^{22}$ [d]
Sapphire, Ruby	~390[f]	3980[f]	~6.2	46[e]	$\sim 1.0x10^{22}$ [f]
Graphite	27[a]	1800[c]	4.6	98[c]	1375[d]
Aluminum	69[a]	2700[a]	3.5	237[c]	2.65[d]
Titanium	116[a]	4500[a]	1.3	21.9[c]	42.0[d]
Stainless Steel	~195[a]	7900[c]	0.4	15[c]	72.0[d]

[a. Ashby and Jones 1980, b. Ashby and Jones 1986, d. Weast and Astle 1980, e. Mills 1992, f. Small Parts Inc. 1993, E and ρ_e for ruby and sapphire are assumed to be approximately equal to the values for alumnina]

TABLE 4.1 Typical properties of possible piston materials. k_T and ρ_e denote thermal conductivity and electrical resistivity

the piston should be at least 1 mm thick. The diameter is contrained by the diameter of the access hole in the base unit. The shape of the front face of the piston remains unknown. If this surface is too pointed, it will dimple the diaphragm upon contact. If the profile is too flat, unreasonable positioning precision is required to ensure that the piston contacts the diaphragm, and not its surroundings. As a conservative estimate of the minimum frontal radius, Brinnell stress analysis was employed. Assuming that the maximum allowable Hertz contact stress for metals is taken to be 1.5 times the yield stress, and that the Poisson ratio for the aluminum piston and the steel plate are identical, it can be shown that [Slocum 1992]

$$R_{min} = \frac{4}{3\,\pi^{1/2}} \left(\frac{1}{1 - \nu^2}\right) \left(\frac{1}{1 + \frac{E_2}{E_1}}\right) \left(\frac{E_2}{\sigma_{y2}}\right) \left(\frac{F}{\sigma_{y2}}\right)^{1/2} \qquad (4.1)$$

where ν, E_1, E_2, σ_{y2}, and F correspond to the Poisson ratio, the Young's Modulus of

aluminum and steel, the yield stress of stainless steel, and the applied force. For $\nu = 0.3$, $E_1 = 69$ GPa, $E_2 = 200$ GPa, $\sigma_{y2} = 310$ MPa, and $F = 10$ N (approximate value from Equation 3.3) shows that $R_{min} \approx 8$ mm. In case positioning proved too difficult, a second set of pistons with $R \approx 5$ mm was manufactured. Both sets were machined on a numerically controlled lathe.

Later in the debugging process, a piston with a frontal radius of 2 to 3 mm was manufactured. It was bonded to the front of the bundle so that no epoxy was placed in between the piezoelectrics and the piston. (See Figure 4.3) This precaution is especially important because the compliance of the epoxy is much greater than that of the actuator. When advanced further than about .05 mm past the point of contact, the piston caused permanent deformation of the diaphragm.

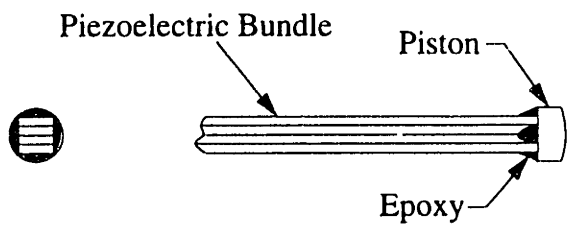

FIGURE 4.3 Attachment of the piston to the front of the bundle

4.4 Chamber Region

As described in Section 3.7, the sensitivities of the governing equations suggest that the geometry of the features on the plates of the chamber region must meet strict

tolerance requirements. With the assistance of Randy Jezowski of RAMCO, Inc. of Salem, Massachusetts, and Dr. Javier Valenzuela of Mikros Manufacturing in Hanover, New Hampshire, the final specifications were refined in light of manufacturing considerations. Using wire electro-discharge machining (EDM) and a numerically controlled high-speed milling machine, the machinists at RAMCO fashioned thin 302 stainless steel plates into the components of the chamber region. The staff at Mikros Manufacturing used a proprietary EDM machine to cut the 50 μm orifice holes, then electro-polished, inspected, and measured the finished components.

A metal-on-metal face seal was used to clamp the plates together. This type of seal was necessary because there is inadequate space for o-ring seats, and thin gaskets introduce unacceptable sources of compliance to the chamber region. The clamp screws moved closer to the chamber with each redesign. In the most recently developed prototype, rules-of-thumb for flexure clamp screw placement [Slocum 1992] were employed. The resulting configuration provided effective sealing and clear optical access to the area at the exit of the orifice.

4.5 Experimental Setup

As shown in Figure 4.4, the experimental setup consisted of the droplet generator, continuous or stroboscopic light sources, a pulse generator, an oscilloscope, a CCD camera with up to 20 times magnification, a video display screen with a reticle generator, an S-VHS video cassette recorder, and a video copy processor. The heated reservoir was attached to the dispenser with a flexible heated hose and could be positioned up to 80 cm above or below the droplet generator.

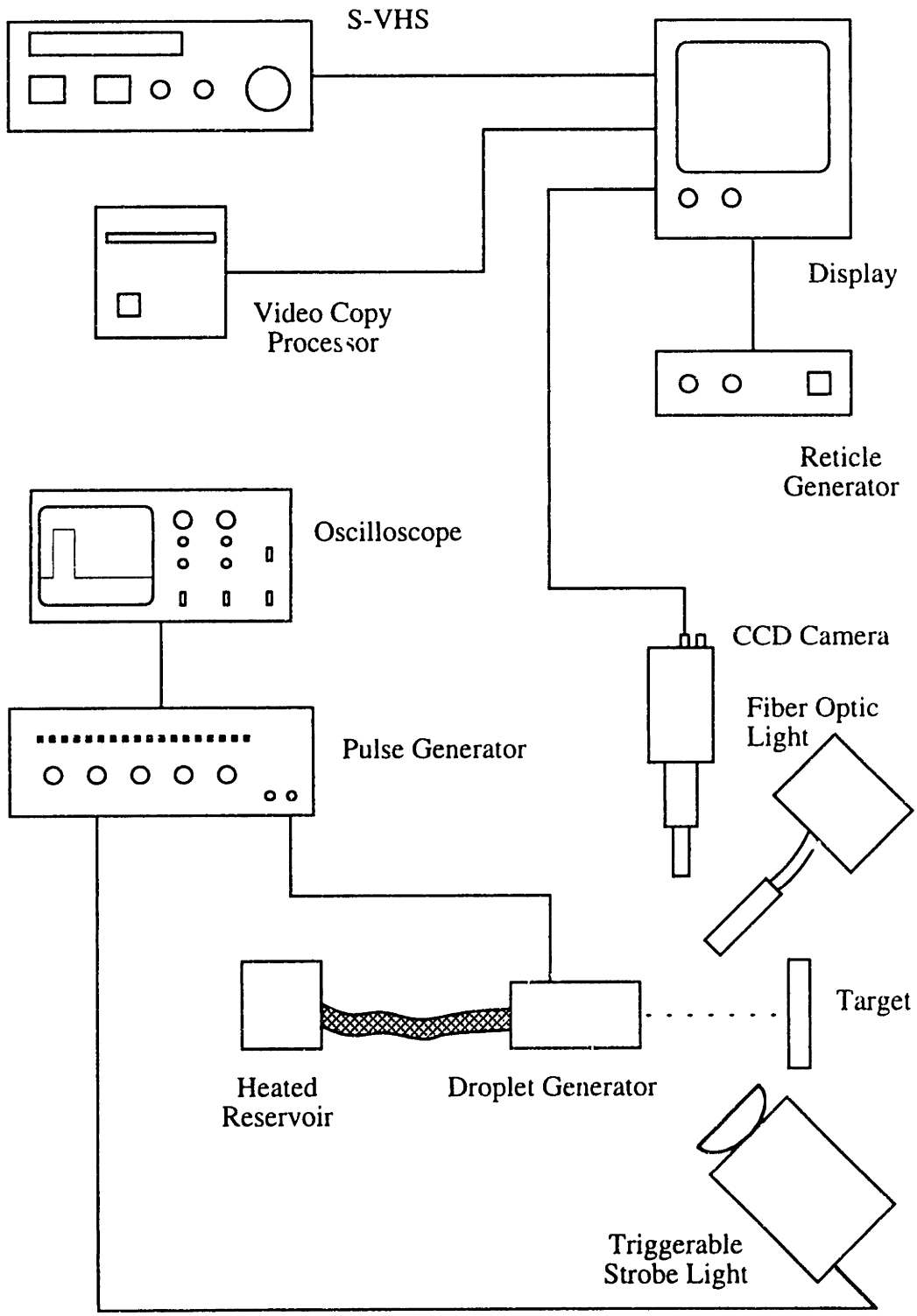

FIGURE 4.4 Experimental apparatus (Adopted from Gao 1994)

CHAPTER 5

Experimental Results and Discussion

5.1 Early Mock-ups of the Proposed Design

To begin exploration of the piezoelectric design concept, mock-ups were constructed using the simplest possible analysis techniques. The modelling of the device pictured in Figure 5.1 assumed that the pressurization of the fluid was a quasi-steady state process occurring in a closed chamber. Without delving into the details of this first analysis, it was shown that an 11 volt applied signal would cause an actuator displacement of one drop volume and the gage pressure in the water would rise to about 11.3 kPa. Using solder as the working fluid, a 25 volt signal would cause the same displacement and the pressure would rise to just over 169 kPa.

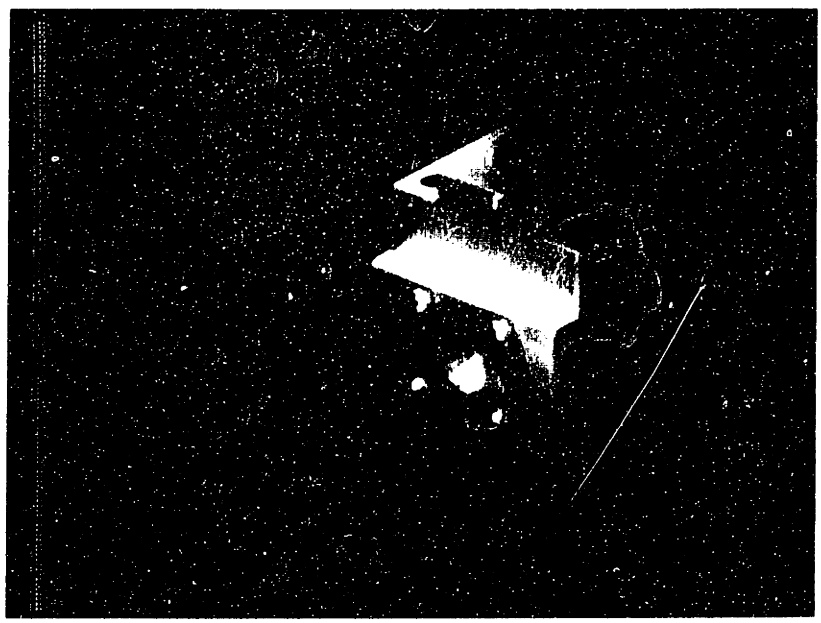

FIGURE 5.1 Photograph of the first mock-up of the piezoelectric design

The device did not eject water droplets. Microscopic study of the meniscus resting in the orifice revealed that the fluid did not move at all during the application of a signal up to 100 volts in magnitude. A solution of Kodak Photoflow was prepared and loaded into the device in an attempt to reduce the likelihood of the presence of bubbles in the chamber. A bilaminar plate (See Figure 5.2) was constructed to increase the theoretical displacement of the driver by 40 times, but still the meniscus remained at rest.

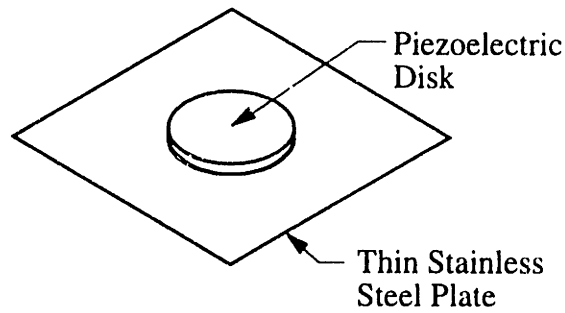

FIGURE 5.2 The bilaminar plate consists of a piezoelectric disk epoxied to the surface of a thin steel diaphragm.

The design did not function as desired due to several factors. Most importantly, the Weber number and volume flow criteria for droplet ejection described in Chapter 2 were not met by the design. The fluid supply ducts were too large in cross section so did not inertially seal the chamber. Furthermore, the complex conical geometry used for the chamber featured many potential nucleation and trapping sites where air bubbles could coalesce.

The second mock-up shown in Figure 5.3 was developed to help improve the restrictor design. In hindsight, the order of magnitude increase in the chamber volume marked a step in the wrong direction. Fluid did issue forth from the orifice when the bilaminar plate actuator was energized, but the exit velocity was so low that the water simply puddled around the exit. The mock-up did not dispense water droplets because the ejection criteria were still not correctly satisfied, but the importance of the inertial sealing of the chamber was now recognized.

FIGURE 5.3 Photograph of the second mock-up

5.2 Clamping Deficiencies of the First Prototype

The prototype shown in Figure 5.4 and 5.5 profited from the experiences with the mock-ups and refinements in the theoretical model. In this design the chamber region was comprised of three steel plates: the diaphragm, the chamber, and the orifice plate. By interchanging rear clamping blocks, either a bilaminar plate or piezoelectric bundle could be tested. The bundle support (not shown in the Figures) is positioned in the X and Y directions by human dexterity and perseverance. The actuator is pushed into Z position using the micrometer head. The droplets exit from the center of the cone cut into the front end clamping block.

The disassembled system was cleaned for approximately 20 minutes in an ultrasonic isopropyl alcohol bath before each experiment was conducted. Attempts to eject water from the system using a single piezoelectric plate were unsuccessful until a thin film of 10,000 c.s. viscosity silicone grease was spread in between each of the plates in the chamber region. Fluid was then forced through the system by manually pressurizing the reservoir. When the driver was fired at frequencies below 30 Hz with a pulse width of approximately 10 μs, a puddle of water about 250 μm in diameter

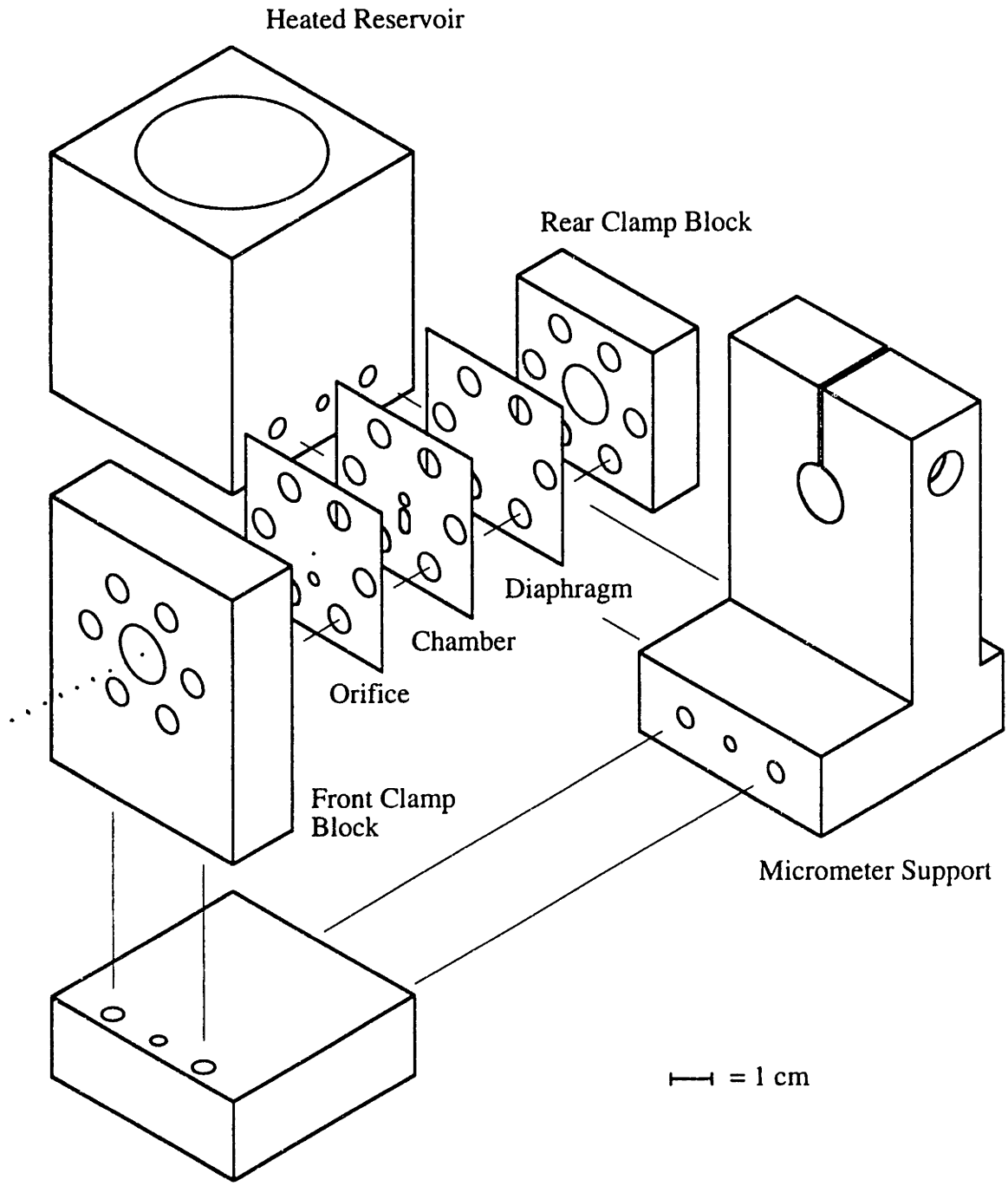

FIGURE 5.4 Assembly drawing of the first prototype

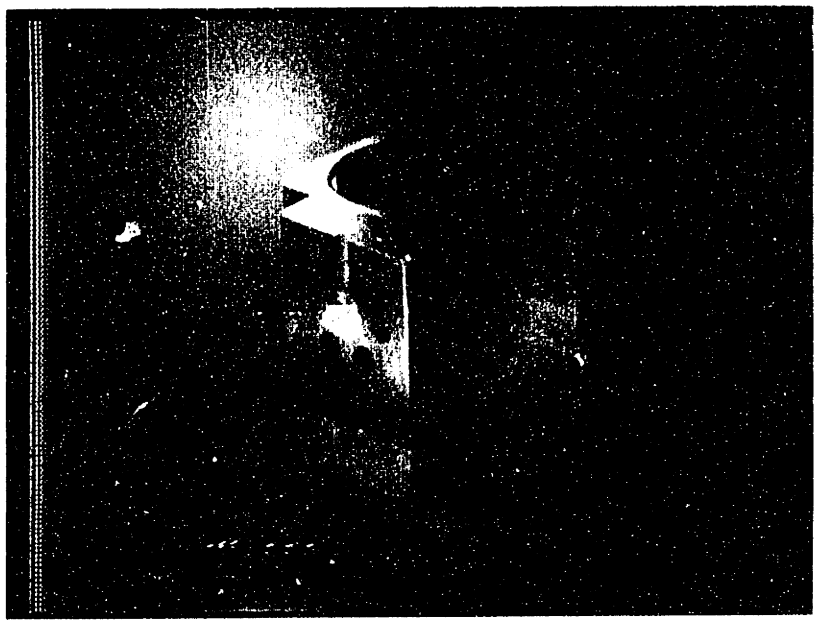

FIGURE 5.5 Photograph of the first prototype

appeared on the outside of the orifice. The size of the puddle oscillated in synch with the input signal. At higher frequencies, the oscillation vanished to the naked eye, but the puddle grew with each applied voltage pulse until the entire orifice area was flooded. Increasing the pulse width while still operating at frequencies above 30 Hz caused the growth rate of the puddle to rise.

Evidently, the high viscosity grease obstructed a leak path or filled a gap between the plates. An atmospheric leak would function similar to the restrictor, so would essentially act as an inertial seal for short time scales. A leak path which connects the chamber back to the supply conduit would cripple performance by effectively enlarging the restrictor. To test for the presence of leaks, an experiment was devised to measure the flow resistance of the restrictor. The experimental value agreed within a factor of two with the theoretical fully-developed flow resistance value.

The most likely site for a gap was between the orifice plate and the machined surface of the front clamp block. Dial indicator measurements of the profile of the rear side of the block revealed that a maximum flatness error of 10 to 30 μm was probable. To experimentally confirm that the measurements of these dimensions were correct, a small drop of water was placed on the outside surface of the otherwise dry orifice plate,

which was clamped tightly to the block. The water quickly seeped into the narrow gap that had thus far escaped observation.

To remedy the flatness error, a film of molten candelilla wax was tightly pressed between the orifice plate and the imperfect clamp block. The assembly was cooled and the wax solidified. The system was again filled with water, and the actuator (now a bundle of four piezoelectric plates) was fired. Using pulse widths ranging from 5 to 30 μs and frequencies from 0 to 10 kHz, the resulting train of water droplets reached a maximum stopping distance of just over 4 cm. The focus of the design effort shifted immediately to solder ejection.

5.3 Air Bubbles and the Second Prototype

In the second prototype shown in Figures 5.6 and 5.7, the chamber and orifice plates were combined to eliminate the possibility of leakage in between the two individual parts. The size of the steel plates was reduced by factor of four, and the clamping screws were moved closer to the chamber to improve sealing. To help position the bundle of piezoelectrics (four double-width ceramic plates were used), a flexural X-Y positioning system was developed. As in the previous design, a non-rotating micrometer head was used to adjust in the Z direction. The geometry of the chamber changed slightly to reflect alterations in the theoretical model.

The revised design successfully ejected water droplets only after the entire system was assembled under the surface of a distilled water bath. Much to the designer's chagrin, this technique proved completely reliable and repeatable over a battery of iterations. The device did aspirate air when driven at frequencies above approximately 5 kHz, or when a strong puff of air was used to clear the orifice area. Typically, the droplets reached their stopping distance after travelling about 3.5 cm. Equation 3.17 indicates that this corresponds to an exit velocity of about 13 m/s, which agrees reasonably well with numerical simulations.

In light of the difficulties experienced in priming the device, additional experiments

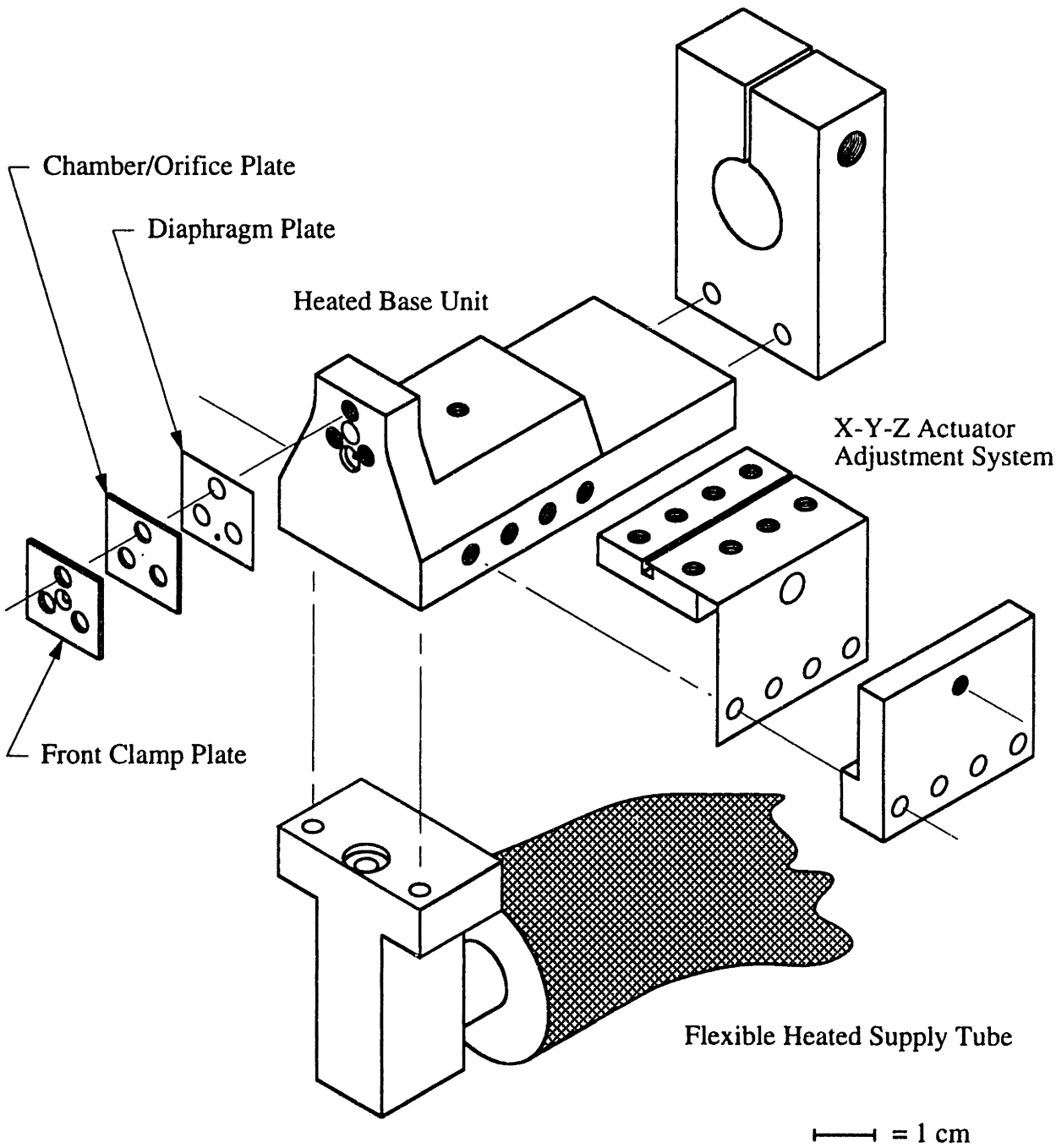

FIGURE 5.6 Assembly drawing of the second prototype

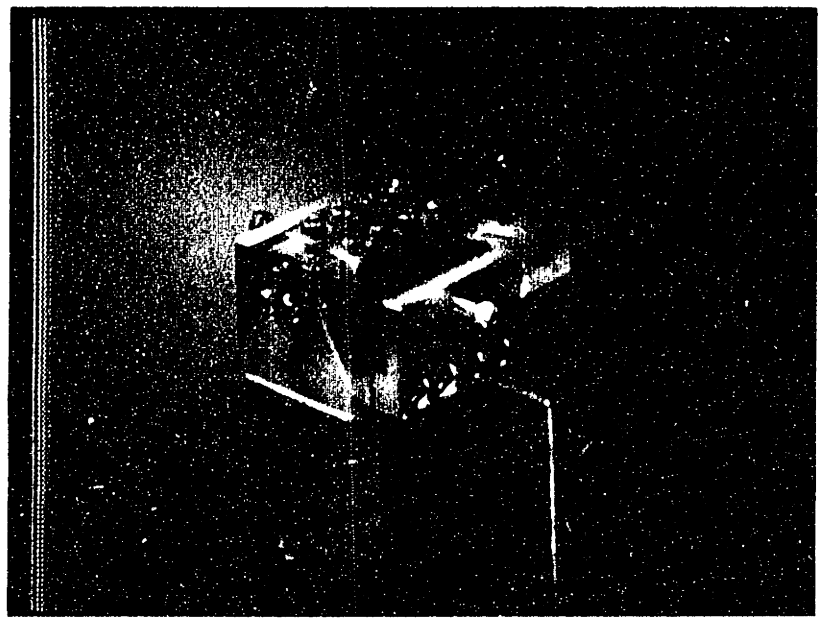

FIGURE 5.7 Photograph of the second prototype

were conducted to study this problem. The steel diaphragm was replaced with a lexan plate to provide optical access to the chamber. The system was manually pressurized and the dynamics of the filling process were studied. Once the fluid wet the orifice, the air remaining in the chamber was trapped. To confirm that this phenomena also occurred for mostly non-wetting fluids, the experiment was repeated after applying a teflon coating to the interior surfaces of the chamber. The same problem was encountered. (See Figure 5.8)

5.4 Moving on to Liquid Metal

To temporarily avoid the complexities of solder oxidation, modified priming schemes were tested using liquid mercury as the working fluid. This substance exhibits physical properties similar to those of solder. (Refer to Table 2.1) Mercury was forced into the system while the clamping screws were not fully tightened, but air still remained trapped at the edges of the chamber. The steel diaphragm was replaced, the priming technique was repeated, and a very interesting result occurred.

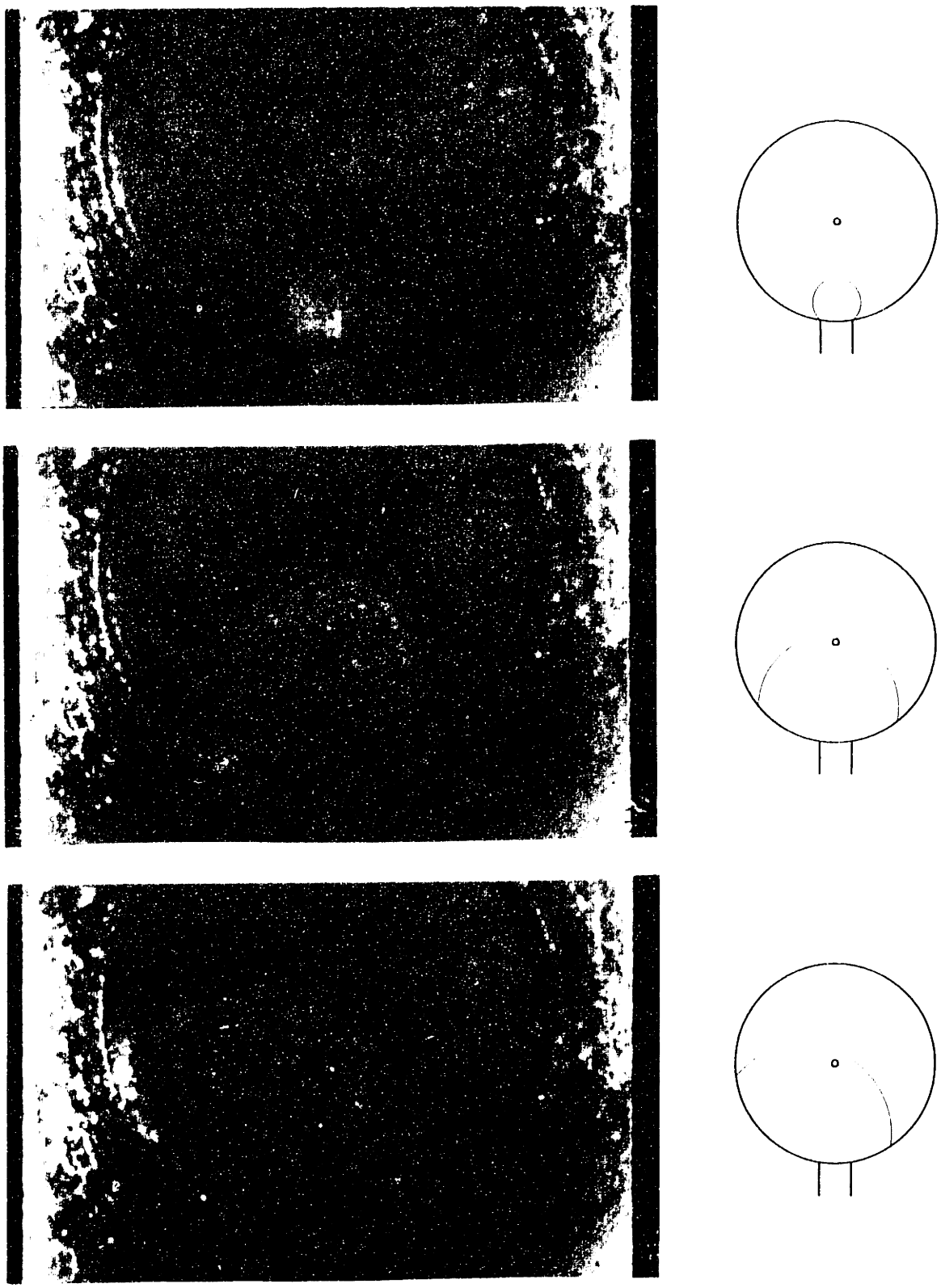

FIGURE 5.8 Dynamic filling sequence showing the trapping of an air pocket in the teflon coated chamber

When driven by a 10 Hz input signal with a pulse width of 10 to 12 μs, a mercury droplet was ejected every two or three pulses. As shown in Figure 5.9, the pulses would incrementally push small volumes of mercury outward until a droplet was finally ejected. It is unclear why the fluid did not retract into the orifice after the first pulses. The "three stage ejection" is considered a very limited success because the droplet volume and flight direction were not repeatable.

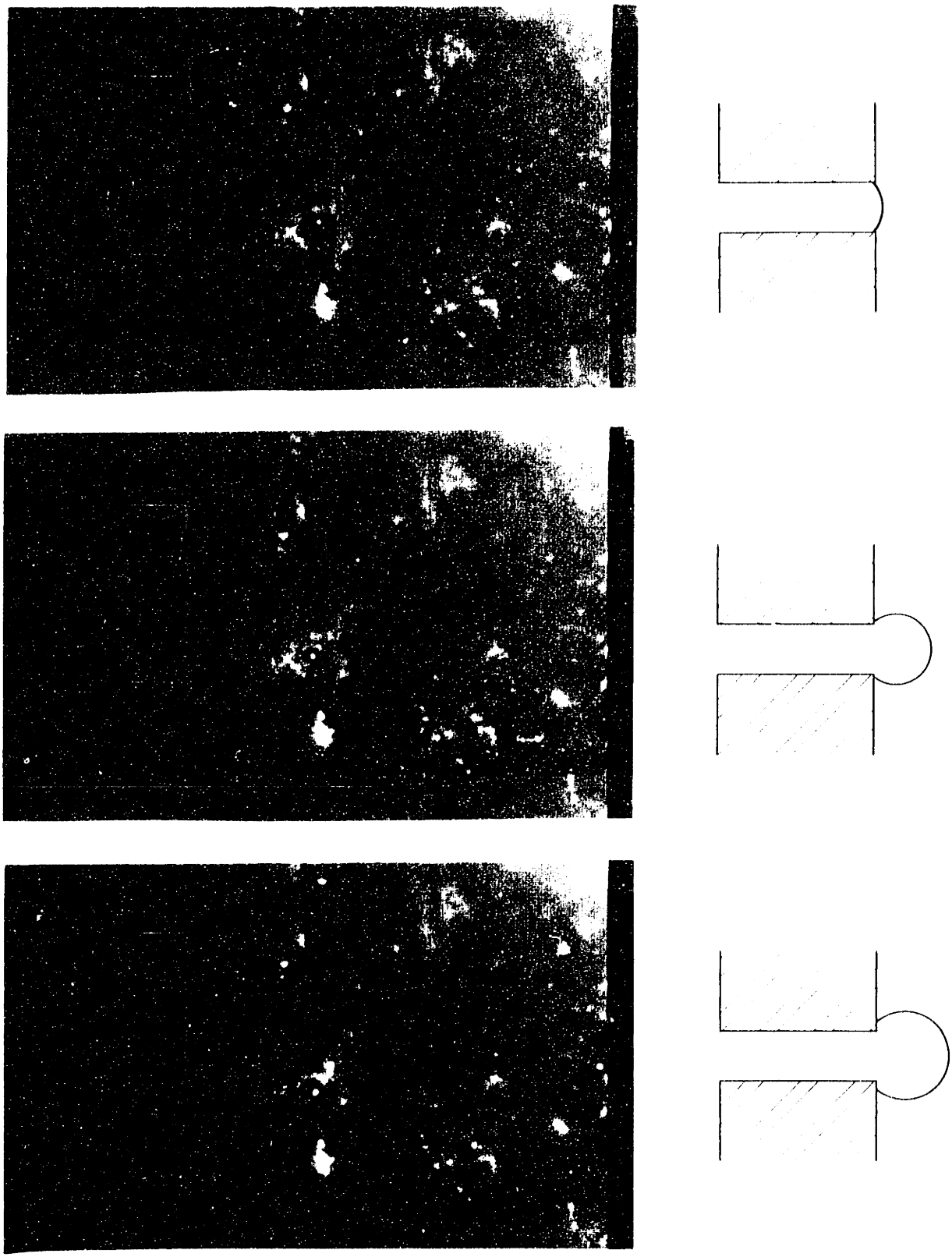

FIGURE 5.9 Dynamic ejection sequence showing the three "stages" leading [illegible] of a single mercury droplet

CHAPTER 6

Conclusions and Future Work

6.1 Conclusions of this Research

Even though attempts to produce droplets of room temperature liquid metal showed very limited success, several important conclusions from this research effort may be drawn. These remarks are loosely divided into theoretical and experimental categories.

A great deal of effort was placed on developing a simple, but adequate, technique for modelling the compression stroke of a drop-on-demand device. This goal was satisfactorily achieved, as the results of the numerical simulations roughly agree with the experimental observations. The actual droplet snap-off phenomenon requires the solution of an unsteady, moving boundary fluid flow problem so is a major research undertaking on its own. However, our simple model is an adequate design tool. With a few minor modifications, the numerical scheme can be extended to the refill phase of operation.

The ejection of liquid metal is theoretically possible, but only marginally so. The model indicates that a sizable bundle of piezoelectric plates can successfully eject a droplet of 50 μm diameter when the applied voltage is greater than about 90 volts. The inaccuracies in the model and the imperfections in the device may mandate the use of a voltage signal larger than the capacity of our existing electronic hardware. The ejection of high temperature liquid metal will also require oxidation protection. This problem has not yet been addressed, but isolating the molten material in, for example, a nitrogen filled enclosure, is fairly straightforward.

The operation of the second prototype showed the absolute necessity of addressing the priming issue during the early phases of the design. The hardware was developed under the assumption that the working fluid would somehow completely fill the chamber and the restrictor. This assumption was unwise, as only submerged assembly in water

yielded satisfactory ejection results. The limited success using liquid mercury suggests, however, that a simple solution may exist, and that the concept developed for molten metal ejection is valid.

6.2 Directions for Future Research

The improvement of the designs described in this work depends upon the ability to make the chamber completely free of air bubbles, or upon the creation of a system which tolerates air bubbles. Removing air from the system requires either a change in the design of the chamber region, or a change in the priming protocol. For instance, the addition of a judiciously placed air vent could facilitate complete chamber filling and still provide effective inertial sealing. The priming technique might be made more effective by using multiple fluids. The device might be filled with an inert, wetting liquid (whose boiling point exceeds the desired operating temperature of the system) before the non-wetting fluid is introduced. This procedure would replace the air pockets with a relatively incompressible liquid. Another promising priming method involves the evacuation of the entire system before filling. Molten solder may be manually forced through the system using pressurized nitrogen. After the liquid metal fills the chamber, the environment around the outside of the orifice may be flooded with nitrogen, thereby ensuring bubble and oxide free operation. The necessary level of vacuum and the possibility of solder vaporization require careful study before attempting this scheme.

In retrospect, it is evident that the air pocket problem can be less severe for different design concepts. The MHD system accelerates the droplet using a localized magnetic pressure in the orifice channel, so a bubble in the reservoir has no effect on the performance of the device. In the extremely unlikely event that a bubble manages to enter the orifice, two important changes occur that affect the subsequent ejection attempt: 1. the current density in the solder remaining in the tube will increase due to the reduced conductor area; and 2. the effective inertial length decreases. Both effects significantly improve the performance of the MHD section, so it is possible that the bubble may be

expelled with the next droplet. A radially contracting piezoelectric tube with the orifice bored through its center enjoys a somewhat similar advantage. Unfortunately, these new designs would have required significant rework effort for us.

This project was intended to develop an understanding of the fundamental physics of molten solder ejection through the design, manufacturing, and testing of a drop-on-demand delivery system. A wealth of knowledge and experience has been acquired through this effort, but only limited success in achieving the goal of solder ejection has been realized. During this study, researchers at Microfab Technologies, Inc. of Plano, TX, [Hayes *et al* 1992] and IBM Personal Computer Company of Austin, TX, [Schiesser *et al* 1994] have developed systems which successfully produce drop-on-demand molten metal droplets of diameter near 50 μm. The systems developed by these companies use piezoelectric and MHD actuation to generate the droplets. In light of these recent developments, the immediate future of the system developed in this work remains uncertain. The background of this project as described in the first Chapter imply that the ejection system is just a small facet of a complex microchip assembly operation. Many more challenges remain unsolved, and many more remain undiscovered.

NOMENCLATURE

α	Expansion coefficient for the piezoelectric bundle. See Equations 3.2 and 3.3.
β	Compression coefficient for the piezoelectric bundle. See Equations 3.2 and 3.3.
β_{ij}	Dielectric coefficient tensor
γ	Volumetric factor which accounts for the curvature of the diaphragm. For our boundary conditions, plate theory shows that $\gamma \approx 1/3$.
δ	Boundary layer thickness
Δt	Time step
ε_{ij}	Strain tensor
η	Kinematic viscosity
θ_d	Dynamic contact angle
θ_o	Static contact angle
κ	Constant used in dynamic contact angle empirical relation. Approximately 1.3×10^{-2} rad^{-3} in magnitude.
κ_s	Isentropic compressibility. $\kappa_s \approx (\rho c^2)^{-1}$ for liquids.
μ	Absolute viscosity
μ_g	Absolute viscosity of the gaseous environment around the ejected droplet
ν	Poisson ratio
ρ	Density
ρ_e	Electrical resistivity
ρ_g	Density of the gaseous environment around the ejected droplet
ρ_i	Density of the liquid in the chamber before compression
σ	Surface tension
σ_{kl}	Stress tensor
σ_y	Yield stress
τ	Characteristic time scale
Φ	Applied voltage
a	Droplet radius
A	Cross sectional area of the chamber
a_o	Orifice radius
A_o	Cross sectional area of the orifice
A_R	Cross sectional area of the restrictor
B	Magnetic field intensity
c	Speed of sound
C_D	Drag coefficient
d/dt	First derivative with respect to time
d^2/dt^2	Second derivative with respect to time
d_{31}	Voltage coefficient for a piezoelectric plate
D_k	Electric displacement vector
D_R	Hydraulic diameter of the restrictor

ds	Notation indicating integration along a streamline
E	Young's modulus
E_i	Electric field vector
f	Function of
F	Applied force
g	Gravitational acceleration
g_{kij}	Voltage coefficient tensor
h	Characteristic dimension of the square orifice used in the MHD system
i	Subscript denoting the current time step
I	Electric current
j	Electric current density
k	Spring constant of the diaphragm as determined by plate theory
k_T	Thermal conductivity
l_s	Stopping distance; distance travelled before the droplet velocity reaches zero.
L	Length of a single piezoelectric plate
L_c	Height of the cylindrical chamber
L_o	Length of the orifice
M	Combined mass of the piston and the diaphragm
N	Number of piezoelectric plates which constitute the actuator bundle
P	Chamber pressure
Q	Heat flux
R	Radius of the piston front
Re	Reynolds number; ratio of inertia to viscous forces
R_{min}	Minimum radius of piston front as determined by Equation 4.1
s_{11}^E	Compliance coefficient for a single piezoelectric plate
s_{ijkl}	Compliance coefficient tensor
t	Time
T	Thickness of a piezoelectric plate
t^*	Time at which the meniscus assumes a hemispherical shape
U	Velocity
U^*	Maximum velocity achievable with the MHD system. See Equation 2.10.
U_o	Velocity of the fluid in the orifice
U_R	Velocity of the fluid in the restrictor
V	Volume
V_{eject}	Volume of fluid ejected from the orifice
V_i	Volume of liquid in the chamber before compression
W	Width of a piezoelectric plate
We	Weber number; ratio of inertial to capillary forces
We_{crit}	Weber number when $t = t^*$
x	Piston position
z	Hydrostatic pressure head
z_o	Position of the liquid in the orifice
z_R	Position of the liquid in the restrictor

REFERENCES

American Piezo Ceramics 1992, *Nominal Characteristics*. Mackeyville, Pennsylvania.

Ando, S., J. Maeda, and K. Fukushima 1981, A New Ink Jet Printing System. *Advances in Non-Impact Printing Technologies for Computer and Office Applications*, J. Gaynor, ed., 1156-1174.

Ashby, Michael F. and David R. H. Jones 1980, *Engineering Materials I*. Oxford: Pergamon Press.

Ashby, Michael F. and David R. H. Jones 1986, *Engineering Materials II*. Oxford: Pergamon Press.

Bird, R. B., W. E. Stewart, and E. N. Lightfoot 1960, *Transport Phenomena*. New York: Wiley.

Bogy, D. B. and F. E. Talke 1984, Experimental and Theoretical Study of Wave Propagation Phenomena in Drop-on-Demand ink Jet Devices. *IBM Journal of Research and Development*. **28** (3), 314-321.

Bugdayci, N., D. B. Bogy, and F. E. Talke 1983, Axisymmetric Motion of Radially Polarized Piezoelectric Cylinders Used in Ink Jet Printing. *IBM Journal of Research and Development*. **27** (2), 171-180.

Darling, Richard H., Chen-Hsiung Lee, and Lawrence Kuhn 1984, Multiple-Nozzle Ink Jet Printing Experiment. *IBM Journal of Research and Development*. **28** (3), 300-306.

Davis, E. M., W. E. Harding, R. S. Schwartz, and J. J. Corning 1964, Solid Logic Technology: Versatile, High-Performance Microelectronics. *IBM Jounral of Research and Development*. **8** (2), 102-114.

Döring, M. 1981, Fundamentals of Drop Formation in DOD Systems. *Advances in Non-Impact Printing Technologies for Computer and Office Applications*, J. Gaynor, ed., 1071-1091.

Edmund Scientific 1995, *Annual Reference Catalog*. Barrington, New Jersey.

Fromm, J. E. 1984, Numerical Calculation of the Fluid Dynamics of Drop-on-Demand Jets. *IBM Journal of Research and Development*. **28** (3), 322-333.

Gao, Fuguan 1994, *Molten Microdrop Deposition and Solidification Processes.* Ph.D. Thesis, Department of Mechanical Engineering, MIT.

Hayes, Donald J., David B. Wallace, and Michael T. Boldman 1992, Picoliter Solder Droplet Dispensing. *ISHM Proceedings.*

Heinzl, J. and C. H. Hertz 1985, Ink-Jet Printing. *Advances in Electronics and Electron Physics.* **65**, 91-171.

Hoffman, Richard L. 1975, A Study of the Advancing Interface. *Journal of Colloid and Interface Science.* **50** (2), 228-241.

Iida, T. and R. Guthrie 1988, *The Physical Properties of Liquid Metals.* Oxford: Clarendon Press.

Kyser, Edmond L., Leland F. Collins, and Nick Herbert 1981, Design of an Impulse Ink Jet. *Journal of Applied Photographic Engineering.*

Kyser, E. L. and S. B. Sears: U. S. Patent 3,940,398.

Lee, F. C., R. N. Mills, and F. E. Talke 1981, Drop-on-Demand Ink Jet Printing at High Print Rates and High Resolution. *Advances in Non-Impact Printing Technologies for Computer and Office Applications*, J. Gaynor, ed., 1059-1070.

Lee, F. C., R. N. Mills, and F. E. Talke 1984, The Application of Drop-on-Demand Ink Jet Technology to Color Printing. *IBM Journal of Research and Development.* **28** (3), 307-313.

Li, Wen-Hsiung, and Sau-Hai Lam 1976, *Principles of Fluid Mechanics.* Reading, Massachusetts: Addison-Wesley.

Miller, L. F. 1969, Controlled Collapse Reflow Chip Joining. *IBM Journal of Research and Development.* **13** (3), 239-250.

Mills, Anthony F. 1992, *Heat Transfer.* Illinois: Irwin.

Piezo Kinetics Incorporated 1993, *Application Notes.* Bellefonte, Pennsylvania.

Piezo Systems Inc. 1994, *Product Catalog 2.* Cambridge, Massachusetts.

Probstein, R. F. and F. Fassio 1970, Dusty Hypersonic Flows. *AIAA Journal.* **8**, 772-779.

Rayleigh, F. R. S. 1878, On the Instability of Jets. *Proceeding of the London Mathematical Society.* **10** (4), 4-13.

Schiesser, Tom, Ed Menard, Ted Smith, and Jim Akin 1994, Micro Dynamic Solder Pump: Drop on Demand Eutectic Solder Dispensing Device. *Proceedings of the Surface Mount International Show.*

Shield, T. W., D. B. Bogy, and F. E. Talke 1987, Drop Formation by DOD Ink-Jet Nozzles: A Comparison of Experiment and Numerical Simulation. *IBM Journal of Research and Development.* **31** (1), 96-110.

Slocum, Alexander H. 1992, *Precision Machine Design.* Englewood Cliffs, New Jersey: Prentice Hall.

Small Parts Inc. 1993, *Fall 1993 Catalog.* **15.**

Stacy, John 1993, Conversations. American Piezo Ceramics. Mackeyville, Pennsylvania.

Stemme, Erik and Stig-Göran Larsson 1972, The Piezoelectric Capillary Injector—A New Hydrodynamic Method for Dot Pattern Generation. *IEEE Transactions on Electron Devices.* **20** (1), 14-19.

Totta, P. A. and R. P. Sopher 1969, SLT Device Metallurgy and its Monolithic Extension. *IBM Journal of Research and Development.* **13** (3), 226-238.

Wallace, David B. 1989, A Method of Characteristics Model of a Drop-on-Demand Ink-Jet Device Using an Integral Method Drop Formation Model. *ASME Society Papers.* 89-WA/FE-4, 1-9.

Weast, Robert C. and Melvin J. Astle, eds. 1980, *CRC Handbook of Chemistry and Physics.* Florida: CRC Press.